國立交通大學

電子工程研究所

碩士學位論文

化學機械研磨之清洗對銅導線電性的研究

Study on Electrical Properties of Cu Interconnect After Post CMP Cleaning

薛國欽

指導教授：葉清發教授
共同指導：羅正忠教授
蔡明蒔博士

中華民國九十三年 六月

摘要

雖然銅導線的化學機械研磨在未來的導線製程上最具潛力的製程，然而卻還有許多待解決問題需要去克服。其中，最大的挑戰爲研磨後的清洗。經過化學機械研磨後，晶圓表面會殘留大量的污染物，包括研磨過程中所使用的研磨粉體、金屬離子等等。若無有效的清洗製程去除這些污染物，則將影響元件特性和製程良率。

當使用含有粉體的研磨漿料作研磨時，粉體會大量吸附在銅導線表面。我們很難利用傳統的清洗方法去除掉。有論文中提出了使用硝酸和 BTA 的混合水溶液進行磨光以去除粉體[1]。在擦光的過程中，藉由硝酸輕微蝕刻去除銅導線表面的之氧化銅鈍化層，而 BTA 將於銅導線表面形成 Cu(Ⅰ)-BTA 保護層以防止氧化銅的生成。但是，此 Cu(Ⅰ)-BTA 保護層會造成表面漏電卻是個未知數。本研究中，將從表面漏電去比較 Cu(Ⅰ)-BTA 保護層和氧化銅鈍化層對表面漏電的影響，氧化銅鈍化層可以代表著傳統銅導線化學機械研磨後銅表面的狀況。在論文中使用 KOH 作爲磨光，然後浸泡雙氧水，以模擬無粉體，但是卻有氧化銅在銅導線表面的情形。除此之外，Cu(Ⅰ)-BTA 保護層的熱穩定性和金屬螯合劑清洗液是否會破壞 Cu(Ⅰ)-BTA 保護層也將在本論文中討論。

銅金屬化學機械研磨後清洗另一關鍵爲去除殘留在介電層表面銅離子。表面殘留大量的銅離子將造成大量的表面漏電[2] [3]。金屬螯合物具有配位基可以和過渡金屬離子形成穩定的錯合物。在本研究中，將探討三種金屬螯何物的清洗效果以及對銅腐蝕的結果。除此之外，清洗溶液若具有好的浸潤能力，則可以確保整個晶圓表面都可以被清洗的很均勻。我們也將討論此三種金屬螯合劑的浸潤能力。同時，也將探討溶液酸鹼度對螯合劑清洗能力的影響。

Abstract

Although Cu CMP has being the enabling technology for multilevel Cu interconnect manufacturing, there were several challenges to its implementation. One of the serious challenges was post-Cu CMP cleaning. There will be a large amount of contaminants on the wafers after Cu CMP, including particles and chemicals from slurry, debris from the substrate which been polished and Cu residuals.

As polishing with colloidal silica based slurry, there was a strong tendency of the absorption of colloidal silica on Cu surface. It was difficult to remove these chemisorbed colloidal silica by conventional chemical clean. A novel process, which was buffing with Nitric acid (HNO_3) and 1H-benzotriazole (1H-BTA, $C_6H_4N_3H$), could remove colloidal silica abrasives from Cu surface [1]. HNO_3 would dissolve Cu oxide layer on Cu surface, while 1H-BTA would coordinate with cuprous ions to form a mono-layer Cu(I)-BTA on the surface to prevent Cu form oxidation. However, one may suspect whether the Cu(I)-BTA layer on Cu surface was stable for thermal and electrical bias stress or not? We would like to explore the mechanism of surface leakage for CuBTA and Cu oxide passivation on Cu surface. Cu oxide on Cu surface could be used to describe the surface condition after conventional CMP. To establish the environment of Cu oxide on the Cu surface without colloidal silica, we used KOH for buffing followed by immersing in hydrogen peroxide (H_2O_2). In additional, thermal stability and chemical durability of CuBTA layer would be discussed in this study.

One of the greatest challenges to the Cu CMP cleaning process was the removal of residual Cu contamination from the dielectric surface. Cu ions remained on the dielectric would cause large leakage current [2] [3]. Metal chelators were known to form stable complexes with Cu ions. Because metal chelators had one or several dentates, they would react as electron-pair acceptors to form coordination

compounds or complex ions with metal ions. The metal chelators in solution would form uncharged Cu-chelator complexes by coordination. In this study, three types of chelotors with different structures would be compared from their cleaning efficiency and corrosion effect. In additional, good wetting ability would ensure whole wafer surface would be coved with chelator chemicals, which made Cu ions cleaning uniformly. We also discussed the wetting ability of chelator solutions in this study. Furthermore, the effect of different pH for chelating capability would be discussed.

誌謝

首先，筆者由衷的感謝指導教授葉清發教授、羅正忠教授與國家奈米元件實驗室蔡明蒔博士兩年來辛勤的指導和教誨，並且在待人處世以及人際關係方面給予莫大的啓發，使我畢生受益匪淺，謹此致以最誠摯的謝意。

筆者亦由衷感謝國家奈米元件實驗室副主任戴寶通博士對於實驗過程以及結果給予莫多的建言。同時感謝國家奈米元件實驗室李美儀小姐、吳柏偉先生、賴明志先生、劉育彬先生等人在實驗上的全力協助。

感謝交大電子所學長蕭智文、王碩晟、陳添富；交大材料所學長方政昱、張簡鵬崇、王寶明；清大微機電所學長蘇旺申在實驗結果分析上給予許多的指教；電子所同學劉俊彥、林榮祥、鐘文駿、林余俊、張志廉、張至揚；清大材料所同學黃秉偉；清大工科所同學黃清鴻逢甲化工同學陳拙聰在求學與研究過程互相鼓勵與提供實驗上的協助。在此特別感謝方政昱學長，由於學長在實驗上的幫助和討論，以及協助解決實驗中所遇到的困難，使的實驗得以順利完成。感謝室友謝政宇、李源興、陳澤許在實驗遇到困難時給予許多的安慰與鼓勵。

感謝國科會國家奈米元件實驗室提供研究設備和實驗材料，本論文才得以完成。亦深深感謝交通大學電子所年來的栽培。最後僅將本論文獻給我摯愛的父母親薛慶成、林慧琦，弟妹薛仁傑、薛依珊，感謝你們的支持和鼓勵使我順利得到碩士學位。

Contents

Table Caption

Figure Caption

Chapter 1

Introduction

1.1 Motivation

1.1.1 Cu Dual Damascene Process and CMP

In semiconductor manufacturing, we always directed toward adding device speed and circuit function. Traditionally, we focused on decreasing feature size to reach this goal, and it really worked. However, in deep sub-micrometer region, the impact of interconnect delay has been beyond intrinsic gate delay (Figure.1-1) [4]. It was obvious that interconnect RC delay would limit the overall chip performance as the technology node below 1 μm. This was due to the resistance of metal lines increased with increasing length and decreasing width. In addition, the parasitic capacitance of metal lines increased with increasing length and decreasing spacing. The interconnect RC delay was given by

$$RC = \rho\varepsilon\frac{l^2}{td} \qquad \text{(Eq.1-1)}$$

where ρ was the resistivity of the metal, ε was the permittivity of the insulator, l and d were length and thickness of the metal line, respectively, and t was the thickness of the insulator [5]. There were three ways to reduce the RC delay. First, introducing multilevel interconnect structure to reduce l and interconnect complexity. Second, introducing low-dielectric constant materials as insulators to reduce ε. Third, introducing low resistivity metals as interconnect materials [4].

Cu as interconnect material could be understood form the view point of material properties. Table.1-1 gave the comparison of properties of several possible interconnect metals [6]. Among these metals, Cu with two primary characteristics of low resistivity (1.7 μΩ.cm) and high melting point(1085

℃) could exhibit good electromigration resistance and reliability. Therefore, Cu was the most promising candidate for the advanced interconnect metallization. However, owing to lack of Cu compounds with high vapor pressure at low temperature, reactive ion etching (RIE) was not practical method to pattern Cu metal lines [7]. Several different methods for fabrication of multilevel Cu interconnect has been reported [8] [9]. The most promising method was known as dual damascene process with chemical mechanical polishing (CMP) (Figure.1-2). Several advantages of dual damascene process using CMP were described below. First, such approach did not need to develop the difficult RIE of copper. Second, the global planarity of surface was achieved by CMP, which means allowing for multilayer stacking of Cu metallization without surface topography buildup[10]. Third, dual damascene process reduced manufacturing process steps and CMP widened the process window [11]. Fourth, Cu CMP was a room-temperature process and this process could reduce the thermal budget. Finally, it was relatively easy to obtain a clean Cu interface after CMP process comparing to metal RIE, which would significantly reduce contact resistance.

1.1.2 Post-Cu CMP Cleaning

Although Cu CMP was a potential process in future multilevel Cu interconnection, there were several challenges to its implementation. One of the serious challenges was post-Cu CMP cleaning. Cu CMP left a large amount of contaminants on the wafers, including particles and chemicals from the slurry, particles from the materials been polished and Cu ion residuals [12].

1.1.2.1 Colloidal Silica Abrasives Removal

During the CMP process, Cu would be oxidized to form Cu oxides (CuO or Cu_2O) and Cu hydroxides ($Cu(OH)_2$) passivation on Cu surface[13]. Then, these passivation on high feature would be polished to reach global planarization, while low feature would not be polished. As polishing with colloidal silica based slurry, it shows the strong absorption of colloidal silica on Cu surface. This might be related to that the colloidal silica chemisorbed on the Cu oxide layer by means of oxygen bridging bonding [14]. It was difficult to remove colloidal silica by conventional chemical clean. In additional, Several papers also indicated this Cu oxide layer was a source of surface leakage [2] [3].

A papers propose a novel process, which was buffing with Nitric acid (HNO_3) and 1H-benzotriazole (1H-BTA, $C_6H_4N_3H$), to remove colloidal silica abrasive [1]. HNO_3 would dissolve Cu oxide layer on Cu surface, while 1H-BTA would coordinate with cuprous ions to form a mono-layer Cu(I)-BTA on the surface to prevent Cu form oxidation(Figure.1-3) [15]. However, one may suspect whether the Cu(I)-BTA layer on Cu surface was stable for thermal and electrical bias stress or not? We would like to explore the mechanism of surface leakage for CuBTA and Cu oxide passivation on Cu surface. Cu oxide on Cu surface could be used to describe the surface condition after conventional CMP. In additional, thermal stability and chemical durability of CuBTA layer would be discussed in this study.

1.1.2.2 Cu Contamination Removal

Besides colloidal silica absorption on the surface, Cu residuals were also source of contamination and were thought to be most deadly. Cu ions were mobile charges which would penetrate into dielectric to form several deep levels in the silicon band gap, which would damage device performance, and likely to lead short between metal lines [2] [3] [5]. As a result, Cu residuals must be clean as far as possible after Cu CMP.

It was a challenge to remove Cu residuals on the dielectrics down to the level less than 5×10^{10} atoms/cm^2 without corrosion to Cu lines [16]. From Pourbaix diagram, it indicated that Cu was corroded in acidic (pH<5) and alkaline (pH>13) solutions easily (Figure.1-4) [4], ammonium hydroxide (NH_4OH) and hydrofluoric acid (HF), which were used for conventional post-oxide CMP cleaning were not suitable for post-Cu CMP cleaning [17]. Especially for NH_4OH, it formed soluble and stable complex Cupric-amine compounds with copper, as shown in (Figure.1-5) [4].

Metal chelators were known to form stable complexes with Cu ions [18]. Because metal chelators had one or several dentates, they would react as electron-pair acceptors to form coordination compounds or complex ions with metal ions. The metal chelators in solution would form uncharged copper-chelator complexes by coordination with metal ions. In this study, three types of chelotors with different structures would be compared from their cleaning efficiency and corrosion effect. In additional, good wetting ability would ensure whole wafer surface would be coved with chelator chemicals, which make Cu ions cleaning uniformly. We also discussed the wetting ability of chelator solutions in this study. Furthermore, the effect of different pH for chelating capability would be discussed.

1.2 Thesis Outline

In this study, we studied the effect of CuBTA layer on surface leakage. We would compare Cu(Ⅰ)-BTA layer with Cu oxide on Cu surface from the view of surface leakage. Cu oxide on Cu surface could be used to describe the surface condition after conventional CMP.

In chapter 2, three types of chelotors would be compared their cleaning efficiency and corrosion effect in this study. In additional, we would explore the influence of pH on chelating Cu ions. Furthermore, wetting ability and corrosion of Cu lines in the cleaning solutions also were discussed.

In chapter 3, we would compare Cu(Ⅰ)-BTA layer with Cu oxide on Cu surface fromed the view of surface leakage. To build the condition of Cu oxide on Cu surface, buffing with KOH also was discussed.

In additional, the thermal stability of CuBTA layer would be discussed.

Finally, conclusions were given in chapter 4.

Chapter 2

Cleaning Efficiency of Chelator Solutions

2.1 Introduction

Although Cu CMP has being the enabling technology for multilevel Cu interconnect manufacturing, there were several challenges to its implementation. One of the serious challenges was post-Cu CMP cleaning. After Cu CMP, Cu contamination presented on the surface in the form of homogeneous film [16]. Cu diffused quickly both in the silicon wafer and in deposited dielectric films. Cu would formed several deep levels in the silicon band gap and acted as recombination centers, which reduced minority carrier lifetime [5]. In additional, Cu residuals on dielectric would form a leaky path and were likely to lead short between metal lines [2][3]. Hence, Cu was considered as a very serious contamination for silicon device and must need to be removed from interlevel dielectrics surface after Cu CMP.

It was a challenge to reduce Cu residuals on the dielectrics to a level less than 5×10^{10} atoms/cm^2 without causing corrosion to Cu lines [16]. Figure.1-4 showed the Pourbaix diagram of Cu-H_2O system. It indicated that acidic solutions(pH<5), Cu oxides did not form and Cu dissolves as Cu^+ at noble (high) potential. On the other hand, in highly alkaline solutions at pH>13, Cu would form $CuO2^-$ at noble potential. Because Cu was corroded in acidic and alkaline solutions easily, ammonium hydroxide (NH_4OH) and hydrofluoric acid (HF) which were used for conventional post-oxide CMP cleaning would be not suitable for post-Cu CMP cleaning [17]. Especially for NH_4OH, it formed soluble and stable complex compounds with Cu, which would corrode the Cu lines seriously as shown in Figure.1-5.

In this study, several metal chelators would be used to remove Cu ions from the interlevel dielectrics surface. Metal chelators were known to form stable complexes with Cu ions [18]. Because metal chelators had one or several dentates, they would react as electron-pair acceptors to form coordination compounds or complex ions with metal ions. The metal chelators in solution would form uncharged Cu-chelator complexes by coordination with metal ions. The removal of Cu contamination from wafer surface by metal chelators could be understood by the distribution equilibrium [19]. The distribution equilibrium could be expressed by the following equations. Metal ions deposited on the wafer surface were dissolved into the aqueous phase (Eq.2-1). The complex reaction occured between metal ion and metal chelator molecule (Eq.2-2). Metal-chelator complex might absorb again on the wafer surface (Eq.2-3). Metal chelator molecule might adsorb on the wafer surface (Eq.2-4).

$$M_{(solid)} \leftrightarrow M_{(aqueous)} \qquad \text{(Eq.2-1)}$$

$$M_{(aqueous)} + L_{(aqueous)} \leftrightarrow ML_{(aqueous)} \qquad \text{(Eq.2-2)}$$

$$ML_{(aqueous)} \leftrightarrow ML_{(solid)} \qquad \text{(Eq.2-3)}$$

$$L_{(aqueous)} \leftrightarrow L_{(solid)} \qquad \text{(Eq.2-4)}$$

where M= metal ion, L= metal chelator, ML= metal-chelator complex, (aqueous)= dissolved in water phase, (solid)= adsorb on the surface.

Three types of chelotors with different structures would be compared from their cleaning efficiency and corrosion effect in this study. Table.2-1 listed the three types of chelator solutions. In the type1, citric acid and ADPA-60 had two dentates. In the type2, EDTA and 422-25S had six dentates. The catechol and TBC were aromatic compounds with a cyclobenzeze.

The pH of chelaors also played important role for chelating capability. We would research the influence of pH on chelating Cu ions. Furthermore, good wetting ability would ensure whole wafer surface would be coved with chelator chemicals, which make Cu ions cleaning uniformly. We would discuss the wetting ability of chelator solutions in this study.

2.2 Experimental

2.2.1 Wetting Ability Test of Chelator Solutions

The substrates were standard 6-inch diameter p-type silicon, (100) orientation wafers. After the standard RCA, about 5500A thick SiO_2 was thermally grown from the silicon substrate in the furnace.

Contact angle test was carried out to decide the wetting ability of chelator solutions. In this study, the concentration of the solutions is $1E^{-2}$ and each drop was fixed at 3ml.

2.2.2 Corrosion Test

The blanket Cu test wafers were stacked Cu/Ta layer structure with a combination thickness of 1000/50 nm which were sputtering deposited onto the p-type, (100) oriented, 6-inch bare silicon wafers with 200 nm thick oxide deposited by PECVD. The PECVD system was STS multiplex cluster system and the sputter system was ULVAC SBH-3308 RDE. The under layer of 50nm Ta was used as an adhesion promoter for the Cu deposition, since Cu did not adhere well on the thermal oxide. It was also used as a diffusion barrier, because Cu was very easy to diffuse into oxide with high diffusivity.

The blanket wafer was immersed into the cleaning chelator solutions for 3 minutes. The concentration of chelator solutions was $1E^{-2}$M. Four point measurement was performed to measure the thickness of Cu films before and after etch respectively and calculate the etch rate, describing in chapter 2.3.

2.2.3 Cleaning Test

2.2.3.1 Sample Preparation

The experiment flow was shown in Figure.2-1. The substrates were standard 6-inch diameter p-type silicon, (100) orientation wafers. After the standard RCA, about 5500A thick SiO_2 was thermally grown from the silicon substrate in the furnace. To make the Cu ions bonded on the oxide layer uniformly without agglomeration, CMP process was used before immersing in 1M $CuSO_4$ for 2 minutes. After CMP process, the surfaces of oxide layers would become fresher and bond with Cu ions easily. The CMP setup is described later in chapter 2.2.3.2. Then, the blanket wafers were cleaned using D. I. Water (DIW) by the post-CMP cleaner of Solid State Equipment Corporation MODE 50 (SSEC-M50). The duration of cleaning was 7 cycles (15 cycles/min) and the rotation rate of wafer was 800 rpm. Then, blank wafers were dry spun at the rotation rate of 2500 rpm.

After preparing the Cu contaminated wafer, the first TXRF analysis was carried out to calculator the amount of Cu ions. Three types of chelator solutions cleaning were performed on the SSEC-M50 cleaner, and following with the second TXRF analysis. Table.2-2 listed the cleaning steps and parameters of SSEC-M50. Then the second TXRF analysis was executed to calculate the cleaning efficiency, describing in chapter 2.3.

2.2.3.2 CMP Process

Polisher Setup

A Westech Model 372M CMP processor (Figure.2-2), consisting of a wafer carrier and a primary circular polishing table mounted with Rodel IC 1400^{TM} grooved (made of polyurethane impregnated polyester) pad and a secondary buffing table mounted with an Rodel Politex Regular E.^{TM} pad, a carrier to hold wafers against the pad, and a Rodel R200-T3 carrier film to provide buff between the carrier and wafer was used for CMP experiments. Recesses in the carrier template mechanically constrain a single

6-inch wafer, preventing it from sliding out from under the carrier during polishing. A polymeric film placed in the recess brought the wafer slightly above the surrounding template surface. When the film was wetted, it provided sufficient surface tension to hold the wafer while it is being positioned over the polishing table. The teflon retaining ring was recessed from the wafer surface about 7 miles. The slurry, pumped out from a reservoir at a controlled rate, was dispensed onto the center of the table. The table and the carrier were both motor driven spindles, rotated independently at constant angular velocities (rpm). The arm was oscillated about their position at half radius of the table to utilize more pad area and to reduce pad wear [20]. Pressure at the wafer-slurry-pad interface was controlled via an overhead mechanism, which allowed pressure to be applied onto the wafer carrier.

Pad Prewet & Pad Conditioning

Pad prewet was performed before the start of each polishing action. The prewet slurry flow rate was at 300 ml/min and the prewet time was fixed at 20 seconds.

Pad conditioning was employed to resurface the pad in order to maintain the removal rate without sacrificing uniformity. The purpose of pad conditioning was to clean the slurry residuals and to lift the pad fiber for further processing. Without this procedure, the polishing rate decreased substantially after several polishing cycles. In our experiments, pad conditioning was done by brush artificially. Pad conditioning was performed before and between each wafer, and polishing was terminated before pad glazing could cause significant reduction in removal rate.

Polishing Recipes & Slurry Formations

The polishing recipes and slurry formulations in cleaning experiment were all listed in the Table.2-3. The commercial SS-25 slurry was colloidal silica abrasive with the size of 30-50 nm approximately. In the phase1, oxide layers were polished to establish the fresher surface and would bond with Cu ions easily. Phase2 is to remove the residual slurry from wafer surface.

2.3 The Performances of Chelator Solutions

Wetting Ability

Information obtained from contact angle provided the fundamental understanding of solid-solid and solid-liquid intermolecular interactions (ex: van-der Waals, acid/base type interations, and electrostatic interations). Considered the drop of a liquid rested on a solid surface. The drop of liquid forming an angle might be considered as resting in equilibrium by balancing the three forces involved. Namely, the interfacial tensions between solid and liquid (γ_{SL}), that between solid and vapor (γ_S) and that between liquid and vapor (γ_L) interface. The equilibrium of three forces and the resulting contact angle was given by the well-known Young’s equation (Figure.2-3) :

$$\gamma_{SL} = \gamma_S - \gamma_L \cos\theta \qquad \text{(Eq.2-5)}$$

where θ was contact angle [21].

Good wetting ability would ensure the whole wafer surface would be coved with cleaning chemicals, which make Cu ions cleaning uniformly. In chelator wetting ability test, contact angle system was KRuSS GmbH and each drop is fixed at 3ml. The concentrations of chelator solutions were $1E^{-2}$.

Cu Film Thickness Measurement

In this study, thickness of the Cu film was calculated by dividing the film resistivity with its measured sheet resistance. The relation between thickness and resistivity was given by

$$\rho = R_s \cdot T \qquad \text{(Eq.2-6)}$$

where ρ is the resistivity (μΩ・cm/□), R_s was the sheet resistance (μΩ/□) and T is the Cu film thickness. We assume that the resistivity of the Cu film was not changed by the processing. The resistivity of Cu film in our experiment was in the range from 1.8 μΩ・cm/□ to 2.3 μΩ・cm/□.

Four point probe system (Napson RT-80/RG-80) was used to measure sheet resistance. For a thin wafer with thickness T much smaller than either a or d, the sheet resistance R_s was given by

$$R_s = CF \cdot \frac{V}{I} \qquad \text{(Eq.2-7)}$$

where CF was the correction factor (Figure.2-4). In the limit when d»S, where S was the probe spacing, the correction factor becomes (π /ln 2)=4.54 [22].

The etch rate of blanket Cu films were calculated by following formula:

$$\text{Etch Rate}= \frac{\text{(Pre-etch thickness)- (Post-etch thickness)}}{\text{Etch time}} \qquad \text{(Eq.2-8)}$$

TXRF Analysis

The total reflection X-ray fluorescence spectrometry (TXRF) could sensitively detect the metallic impurities on surface. In this study, the Cu contamination on the dielectric surface was detected using an ATOMIKA 8030W TXRF system. TXRF was based on the photoelectric effect. When an atom irradiated with highly energetic photons, an electron from one of the inner shells might be ejected. As the vacant place was filled by an electron from an outer shell, a photon whose energy was characteristic of the atom was released. This radiation was called fluorescent radiation and detected by an energy dispersive detector. TXRF made use of total reflection of the primary X-ray beam at grazing incidence (Figure.2-5) [23] [24]. The high reflectivity in the total reflection mode resulted in an extremely low energy transfer from the incident beam into the irradiated substrate, because most of the energy was reflected and does not penetrate through the interface.

In this study, TXRF was used to decide the amount of Cu ions. The cleaning efficiency was gave by

$$\text{Cleaning Efficiency}=\frac{[\text{amount of Cu ions before chelators cleaning}]}{[\text{amount of Cu ions after chelators cleaning}]} \qquad \text{(Eq.2-9)}$$

Electrochemical Analysis

Figure.2-6 depicted a typical electrochemical corrosion test cell consisting of three electrodes submerged in an electrolyte. Electrical current form a potentiostat changed the test electrode potential from its open circuit potential (OCP), to a potential value that was determined by the magnitude of potentiostat current. Test electrode polarization was measured as a potential difference between reference and test electrodes. No electrical current flowed between a potentiostat and reference electrodes, so it remained at its OCP and provided a fixed reference point for corrosion measurement. The reference electrode was also used provide feedback to the potentiostat, so that test electrode potential could be monitored and adjusted to a desired level [25].

In this study, electrochemical analysis was used to describe the corrosion behavior of chlators with different pH. All electrochemical analyses were carried out in a conventional three-electrode system at room temperature. A platinum electrode was used as the counter electrode, and an Ag/AgCl was employed as the reference electrode. A Cu cylinder was used as the working electrode, and area of cross section is 0.5 cm^2.

2.4 Results and Discussions

2.4.1 Wetting Ability and Corrosion of Chelotor Solutions

The wetting ability of metal chlators was investigated by contact angle measurement. The results were shown in Table.2-4. The concentration of the solutions is 1E^{-2} and each drop was fixed at 3ml. Table.2-4 indicated that all three types of chelator solutions had low contact angles, which implied good wetting ability. Good wetting ability ensured whole wafer surface would be coved with chelator chemicals, which make Cu ions cleaning uniformly around the wafer..

Figure.2-7 showed the corrosion effect of chelator solutions for Cu films and the formula was shown in Eq.2-8. The concentration of the solutions is 1E^{-2} M and etch time was 3 minutes. It indicated that all three types of chelater solutions had low corrosion rate, even in high concentration.

2.4.2 Cleaning Efficiency of Chelator Solutions

Figure.2-8 and Figure.2-9 showed the results of cleaning efficiency. The calculating formula was showed in Eq.2-9, which the amount of Cu ions before chelators cleaning ranged about from 170×10^{10} to 200×10^{10} atoms/cm^2. As shown in Figure.2-8, the cleaning efficiency would be saturated after 15 cycles (15 cycles/min) cleaning time for all kinds of cleaning solution. EDTA had six strong potential sites for bounding with Cu ions: the four carboxyl groups and the two amino groups, hence EDTA had the best cleaning efficiency. On the contrary, Catechol and TBC had only two dentates and exhibited the worse cleaning efficiency. The cleaning efficiency was strongly dependent on the numbers of chelating sites.

Figure.2-9 indicated the concentration of chelators only had little influence on cleaning efficiency. The low concentration of chelators had enough ability to cleaning the most Cu ions. The other Cu ions could not be chelated, even in high concentration of chelators. This indicated chelators could be used for cleaning with low concentration to decrease budget.

2.4.3 pH Effect on Cleaning Efficiency

The pH of cleaning solutions would influence chelating capability owing to the varying activing of protonated or deprotonated functional groups. For a metal chelator, Y, the chelating reaction for a metal ion M could be represented as [26]:

$$M + Y \leftrightarrow MY$$

$$\beta \; H^{+}$$

$$HY, H_2Y, H_3Y, ... \qquad \text{Eq.2-10}$$

when the Eq.2-10 reached equilibrium state, the total concentration of Y which did not complex with metal ions was given by:

$$c_Y = [Y] + [HY] + [H_2Y] + [H_3Y] + ... \qquad \text{Eq.2-11}$$

The concentration of Y in the solution was given by:

$$\alpha_Y = \frac{[Y]}{[c_Y]}$$

$$= \frac{[Y]}{[Y] + [HY] + [H_2Y] + [H_3Y] + ...}$$

$$= \frac{1}{1 + \frac{[HY]}{[Y]} + \frac{[H_2Y]}{[Y]} + \frac{[H_3Y]}{[Y]} + ...} \qquad \text{Eq.2-12}$$

The proton equilibrium-constant was given by

$$\beta_n = \frac{[H_nY]}{[Y][H^+]^n} \qquad \text{Eq.2-13}$$

$$\frac{[H_nY]}{[Y]} = \beta_n [H^+] \qquad \text{Eq.2-14}$$

Substituting Eq.2-14 into Eq.2-12, the expression of α_Y could now be written as:

$$\alpha_{Y(H)} = \frac{1}{1+\sum_{i=1}^{n}\beta_i[H^+]^i} \qquad \text{Eq.2-14}$$

A high value of α_Y was always desirable for achieving good chelating capability. This was achieved, according to Eq.2-14, at a high pH of cleaning solutions.

In this study, type1 of chelators was taken for experiment and KOH was used to modify the pH of chelator solutions. Figure.2-10 and Figure.2-11 showed the cleaning efficiency of citric acid with various cleaning times and various concentration, respectively. Both Figure.2-10 and Figure.2-11 showed citric acid in the acidic environment had better cleaning efficiency than in the alkaline environment, but it did not agreed with Eq.2-14. ADPA-60 had the same result with citric acid as shown in Figure.2-12 and Figure.2-13. It might be due to that Cu was oxidized to Cu oxide in the alkaline environment. Chelators could not chelate those Cu oxide, hence the cleaning efficiency reduce in the alkaline environment. The Pourbaix diagram indicated that CuO formed between pH=7 to pH=13 at noble (high) potential and Cu_2O formed between pH=5 to pH=15 at active (low) potential as shown in Figure.1-4. Figure.2-14 indicated the etch rate of citric acid in the alkaline environment lower than in the acidic environment, which also implied the passivation appeared in the alkaline environment. In additional, Tafel diagram as shown in Figure.2-15 indicated that surface passivationon Cu formed in the alkaline environment. ADPA-60 had the same phenomenon with citric acid in the alkaline environment as shown in Figure.2-16 and Figure.2-17. It was reasonable to presume that all three types of chelators had the lower cleaning efficiency in the alkaline environment than in the acidic environment, because Cu was oxidized to Cu oxide in the alkaline environment.

2.5 Summary

In this study, we discussed several effects on cleaning efficiency of three types of clelators. All three types of chelator solutions had low contact angles, which implied good wetting ability. Good wetting ability ensured whole wafer surface would be coved with chelator chemicals, which made Cu ions cleaning uniformly around the wafer. In additional, chelater solutions had low corrosion rate for Cu lines, even in high concentration.

The cleaning efficiency was strongly dependent on the numbers of chelating sites. EDTA had six strong potential sites for bounding with Cu ions: the four carboxyl groups and the two amino groups, hence EDTA had the best cleaning efficiency. On the contrary, Catechol and TBC had the fewest dentates and showed the worse cleaning efficiency. Besides, chelator solutions in the alkaline environment were improper for cleanig, because Cu was oxidized to Cu oxide in the alkaline environment. Chelators could not chelate those Cu oxide, hence the cleaning efficiency reduced in the alkaline environment.

Chapter 3

Effect of CuBTA Layer on Surface Leakage

3.1 Introduction

The damascene process was regarded to be the an essential and critical step for manufacturing Cu interconnect, and the chemical mechanical polishing of Cu and barrier metal was the key to enable this process. There were several CMP issues which should be taken into account for implement metal polishing—non-uniformity, rounding, dishing, and erosion—had also been addressed. In order to provide damascene metal lines with high accuracy and yield, a two step CMP had been introduced to achieve a large removal rate while suppressing metal dishing (Figure.3-1). The performance of the second step polishing was to remove the barrier metal selectively. Whatever the degree of dishing during the first step was, if the removal rates of tantalum (barrier metal) and oxide (interlevel dielectric) higher than that of Cu, it was able to reduce both the dishing and oxide erosion within the accepted range in the second step. It had been demonstrated that the slurry composed of colloidal silica abrasive and H_2O_2 could satisfy the demands of the second step polishing.

During the CMP process, Cu would be oxidized to form Cu oxides (CuO or Cu_2O) and Cu hydroxides ($Cu(OH)_2$) passivation on Cu surface[13]. Then, these passivation on high feature would be polished to reach global planarization, while low feature would not be polished. As polishing with colloidal silica based slurry, it shows the strong absorption of colloidal silica on Cu surface. This might be related to that the colloidal silica chemisorbed on the Cu oxide layer by means of oxygen bridging bonding [14]. It was difficult to remove colloidal silica by conventional chemical clean. In additional, Several papers also indicated this Cu oxide layer was a source of surface leakage [2] [3].

A novel process, which was buffing with Nitric acid (HNO_3) and 1H-benzotriazole (1H-BTA, $C_6H_4N_3H$), could remove colloidal silica abrasives from Cu surface [1]. HNO_3 would dissolve Cu oxide layer on Cu surface, while 1H-BTA would coordinate with cuprous ions to form a mono-layer Cu(I)-BTA on the surface to prevent Cu form oxidation (Figure.1-3) [15]. There were two types of Cu(I)-BTA grew on Cu surface. Cu(I)-BTA film grew on the oxygen reconstructed Cu surface in the amorphous-like type. On the other hand, Cu(I)-BTA film would form mono-layer on the clean Cu surface[27]. Because of the existence of HNO_3, there would be no any Cu oxide adsorbed on the Cu surface indicated in Figure.1-4. Hence, 1H-BTA would coordinate with Cu to form a mono-layer Cu(I)-BTA on the Cu surface during buffing with HNO_3/1H-BTA.

One may suspect whether the Cu(I)-BTA layer on Cu surface was stable for thermal and electrical bias stress or not? We would like to explore the mechanism of surface leakage for CuBTA and Cu oxide passivation on Cu surface. Cu oxide on Cu surface could be used to describe the surface condition after conventional CMP. In additional, thermal stability and chemical durability of CuBTA layer would be discussed in this study.

3.2 Experimental Procedures

3.2.1 Chemical Durability of Cu-BTA Passivation in Cleaning Solutions

The blanket Cu test wafers were stacked Cu/Ta layer structure with a combination thickness of 1000/50 nm which were sputtering deposited onto the p-type, (100) oriented, 6-inch bare silicon wafers with 200 nm thick oxide deposited by PECVD. The blanket Cu wafer was immersed into the HNO_3/BTA solution to form CuBTA passivation on Cu surface. The concentrations of HNO_3/BTA were $0.6/1E^{-3}$M and the immersing time was 3 minutes. After that, the wafers were immersed into cleaning solutions for 3 minute. To evaluate the existence of CuBTA on Cu surface after immersing with cleaning solutions, contact angle test and ESCA analysis were perform to evaluation the effect of chelator solution on CuBTA.

3.2.2 Thermal Stability of CuBTA

The blanket Cu test wafers were stacked Cu/Ta layer structure with a combination thickness of 1000/50 nm which were sputtering deposited onto the p-type, (100) oriented, 6-inch bare silicon wafers with 200 nm thick oxide deposited by PECVD. The blanket wafer was immersed into HNO_3/BTA to form CuBTA passivation on Cu surface. The concentration of HNO_3/BTA was $0.6/1E^{-3}$M and the immersing time was 3 minutes. After that, the blanket wafers were baked on the hot plate for 10 minutes. Contact angle and ESCA analysis were performed to evaluation the temperature effect on CuBTA.

The blanket Cu film could not use to perform TDS analysis, because Cu film would reflect infrared ray used to rise temperature. To carry out TDS analysis, the pattern Cu test wafers were stacked Cu/Ta layer structure with a combination thickness of 1000/50 nm using shield mask. The pattern wafer was immersed into HNO_3/BTA to form CuBTA passivation on Cu surface. The concentration of HNO_3/BTA was $0.6/1E^{-3}$M and the immersing time was 3 minutes. Following that, TDS analysis was performed.

3.2.3 Surface Morphology after Buffing

The blanket Cu test wafers were stacked Cu/Ta layer structure with a combination thickness of 1000/50 nm which were sputtering deposited onto the p-type, (100) oriented, 6-inch bare silicon wafers with 200 nm thick oxide deposited by PECVD. The polishing setup was described in chapter 2.2.3.2. The polishing recipes and slurry formulations were all listed in the Table.3-1. After 1st polishing, buffing with

KOH or HNO_3/1H-BTA was used to remove colloidal silica. Blank wafers were dry spun at the rotation rate of 2500 rpm following buffing. AFM was used to evaluate surface morphology after KOH and HNO_3/BTA buffing.

3.2.4 Evaluating Passivation Effect on Surface Leakage Current

The experiment flow was shown in Figure.3-2. To establish the environment of Cu oxide on the Cu surface without colloidal silica, we used KOH for buffing followed by immersing in hydrogen peroxide (H_2O_2). The polishing setup was described in chapter 2.2.3.2. The polishing recipes and slurry formulations were listed in the Table.3-2. The wafer were cleaned using the post-CMP cleaner of Solid State Equipment Corporation MODE 50 (SSEC-M50). Table.3-3 listed the cleaning steps and parameters of SSEC-M50. The comb structure (Figure.3-3) was used to evaluate the surface leakage current and the linewidth/space is 0.8/0.8 μm. The substrates were standard 6-inch diameter p-type silicon, (100) orientation wafers. After the standard RCA, about 1.5 μm thick SiO_2 was thermally grown from the silicon substrate in the furnace. The desired metal pattern was transferred into the SiO_2 layer by means of g-line optical lithography and reactive ion etching. The trenches were etched to a depth 900nm. The photoresist was ashed within ozone ambient and followed by a 125℃ H_2SO_4/H_2O_2 stripping. The wafers were then deposited a 50 nm thick layer of Ta, followed by a 1,700nm thick Cu film by sputtering. After sample preparing, bias temperature stress (BTS) measuring was carried out on the HP4156. The temperature and voltage of stress are 100℃ and 100V, respectively. After stress, the temperature was descended to room temperature. Following that, surface leakage current was measured.

3.3 The Performances of Experimental

Contact angle

The concept of contact angle was shown in chapter.2.3. In this chapter, the use of water drop was for the purpose of fixing the γ_L(Figure.2-3) and each water drop was 3ml.

AFM Analysis

In order to evaluate the practicability of HNO_3/BTA buffing and KOH buffing for removing colloidal silica abrasives on the polished Cu surface, atomic force microscope (AFM) was employed to scould a 10μm×10μm area of Cu surface. In AFM, a fine tip scouldning on the substrate measured surface morphology and properties through an interaction between the tip and surface. In the used measuring mode commonly, the distance between the tip and sample surface was kept constant by a feedback loop during the measurements. There were three operation modes of the AFM (Digital Instruments DI 5000) used to measure the SAM surface quality. From the image resolution viewpoint, contact mode scanning was the best but it would damage the sample surface. Hence, the tapping mode scanning of the AFM was used to measure the surface morphology in this study.

ESCA Analysis

ESCA was based on the photoelectric effect. When a solid was exposed to a flux of X-ray photos of known energy, photoelectrons were emitted from the solid. This photoelectron was emitted with a kinetic energy characteristic of the difference between the X-ray and binding energy of the electron. The energy of the emitted photoelectron defines the type of atom, and the number of photoelectrons at this energy was related to the number density of atoms present. A schematic drawing of a typical ESCA spectrometer was show in Figure.3-4 [28]. ESCA analysis was performed on Americould Physical Electronics ESCA PHI 1600 with Al anode (1486.6 eV).

In this study, electron spectroscopy for chemical analysis (ESCA) was employed to analysis the existence of Cu(Ⅰ)-BTA. Cu(Ⅰ)-BTA has C、Cu、N atoms, but C atoms polluted wafers easily from air or hand-touch contamination. Hence, we observed N atoms to distinguish if BTA coordinate with Cu^+ ion on the Cu surface.

TDS Analysis

Thermal Desorption Spectroscopy (TDS, Hitachi Tokyo Electronics) was a mass analysis apparatus by heating the sample while contained in N_2 or Ar and simultaneously detecting the trace of out-gassing species transferred by carrier gas (N_2 or Ar) from the sample. As the temperature rises, not only absorbed or trapping species, but also the decomposed products of the substrate could be out-gassing species and they would be detected as a rise in ion intensity for a certain mass. This resulted in a specific-mass peak of the out-gassing species intensity versus temperature plot. The temperature at the maximum out-gassing mass peak would be related to the thermal activation energy for desorbing or decomposing reaction. Hence, the thermal stability of Cu(Ⅰ)-BTA could be evaluated by the mass detecting.

When 1H-BTA ions coordinated with Cu^+ to form a mono-layer of Cu(Ⅰ)-BTA, it would cut H atom off (Figure.1-3). We would observe the peak of mass 118 to decide that if Cu(Ⅰ)-BTA exist on wafer surface or not in this study, because the mass of 1H-BTA is 119.

3.4 Results and Discussions

3.4.1 Chemical Durability of CuBTA

The results of contact angle after cleaning of chelator solutions were shown in Table.3-4. It was obvious that Cu film was hydrophilic and CuBTA layer was hydrophobic. After immersing of chelator solutions, the Cu film still was hydrophobic except after citric acid immersing. The contact angle was 53° , which was close to the contact angle of Cu film, after immersing into citric acid. It is likely that CuBTA were destroyed after citric acid immersing. ESCA analysis of Figure.3-5 illustrated there was no peak of N after immersing into citric acid, which meant that CuBTA disappeared after immersing into citric acid. Furthermore, the results of contact angle after cleaning of modified citric acid were shown in Table.3-5 and Figure.3-6. KOH was used to adjust pH of citric acid. It was obvious that CuBTA layer would be destroyed after immersing into higher concentration and lower pH of citric acid. In the latter experiment of evaluating passivation effect on surface leakage current, 1E-3M citric acid would be used to clean wafer after CMP process to prevent damaging CuBTA.

3.4.2 Thermal Stability of CuBTA

The temperature beyond 150℃ would destroy the CuBTA layer shown in Figure.3-7. The contact angle of BTA layer with temperature treatment of beyond 150℃ was lower than the contact angle of 48.5℃ of pure Cu film (shown in Table.3-4). TDS analysis of Figure.3-8 also showed that mass of 118 appeared beyond temperature of 150℃, which meant that CuBTA layer was destroyed. The Cu peak of ESCA analysis showed the bigger satellite peak with higher temperature shown in Figure.3-9(b). In additional, there were no N peak of ESCA analysis shown in Figure.3-9(c). This indicated that CuBTA layer was destroyed and oxidation progressed gradually with high temperature [29]. The N peak of ESCA analysis showed the N peak disappeared at 200℃, which indicated that CuBTA had destroyed. It confirmed that CuBTA film would been destroyed at the range of about 150℃ to 200℃.

3.4.3 Surface morphology after buffing

To build the condition of Cu oxide on Cu surface to describe the surface condition after conventional CMP, KOH was used for buffing in this study. AFM wad used to characterize the surface morphology after buffing to check if buffing with KOH remove colloidal silica or not. The AFM analysis of buffing with HNO_3/1H-BTA showed in Figure.3-10. As shown, a clean Cu surface was observed after buffing with HNO_3/1H-BTA, which agreed with the result in the thesis of Po-Lin Chen [1]. The AFM analysis of buffing with KOH was shown in Figure.3-11 to Figure.3-14. As shown, buffing with KOH could remove colloidal silica. However, the concentration of KOH and polishing time of buffing would dramatically influence the roughness of polished Cu surface. Buffing with 1M KOH for 3 minutes could bring about the cleanest surface and the least roughness. In the latter experiment of evaluating passivation effect on surface leakage current, buffing with 1M KOH for 3 minutes would be used to control the condition of Cu oxide on Cu surface.

3.4.4 Evaluating Passivation Effect on Surface Leakage Current

Mechanism of dielectric degradation between Cu interconnects and schematic band diagram were shown in Figure.3-15 [30]. After the Cu CMP process, the Cu surface was oxidized. In the surface layer of Cu oxide, some Cu atoms were ionized and easily moved into the SiO_2 interface. Also, the SiO_2 surface was severely damaged during CMP process, and dangling bounds were likely to form near the interface. Therefore, the key to reduce interface leakage current was to eliminate Cu oxide formation.

CuBTA on Cu surface could prevent Cu oxide from growing, hence it reduced surface leakage current, shown in Figure.3-16. However, after BTS, the leakage current of CuBTA on Cu surface increased. The high temperature would degrade the CuBTA layer as described formerly, hence, Cu oxide would grow on Cu surface, which cause bigger leakage current. Although the high temperature would degrade the CuBTA layer, the leakage current also was smaller than that of Cu oxide on Cu surface. In additional, Cu oxide on Cu surface made the distribution of leakage current non-uniform around the wafer. This was because that Cu oxide grew non-uniformly around the wafer.

3.5 Summary

In this study, CuBTA layer on Cu surface would reduce surface leakage was proven. To build the condition of Cu oxide on Cu surface, buffing with KOH was discussed. In additional, to prevent damaging CuBTA layer, chemical durability of CuBTA layer also was discussed in this study. 1E-3M citric acid was used to clean wafer after CMP process to prevent damaging CuBTA. CuBTA on Cu surface could prevent Cu oxide from growing, hence it reduced surface leakage current. However, after BTS, the leakage current of CuBTA on Cu surface increased. The high temperature would degrade the CuBTA layer as described, hence, Cu oxide would grow on Cu surface, which cause bigger leakage current. Thermal stability of CuBTA also was discussed in this study. CuBTA film would been decomposed at the range of about 150℃ to 200℃. Although the high temperature would degrade the CuBTA layer, the leakage current also was smaller than those without Cu-BTA but oxide passivation.

Chapter 4

Conclusions

In this study, we studied the effect of CuBTA layer on surface leakage. At first, the cleaning efficiency of Cu ions on the dielectric of three types of chelator solutions was discussed. Metal chelators are known to form stable complexes with copper ions. Because metal chelators had one or several dentates, they would react as electron-pair acceptors to form coordination compounds or complex ions with metal ions. All three types of chelator solutions had low contact angles, which implied good wetting ability. Good wetting ability ensured whole wafer surface would be coved with chelator chemicals, which made copper ions cleaning uniformly around the wafer. Besides, chelater solutions had low corrosion rate for Cu lines, even in high concentration. The cleaning efficiency was strongly dependent on the numbers of chelating sites. EDTA had six strong potential sites for bounding with copper ions: the four carboxyl groups and the two amino groups, hence EDTA had the best cleaning efficiency. On the contrary, Catechol and TBC had only two dentates and showed the worse cleaning efficiency. In additional, the effect of pH of chelator solution were discussed. Chelator solutions in the alkaline environment were improper for cleanig, because copper was oxidized to copper oxide in the alkaline environment. Chelators could not chelate those copper oxide, hence the cleaning efficiency reduced in the alkaline environment.

HNO_3/1H-BTA and KOH were used for buffing to remove colloidal silica. HNO_3 would dissolve copper oxide layer on copper surface, while 1H-BTA would coordinate with Cu to form a mono-layer Cu(Ⅰ)-BTA on the surface to prevent copper form oxidizing. KOH for buffing followed by immersing in H_2O_2 was to establish the environment of copper oxide on the copper surface without colloidal silica. CuBTA layer on Cu surface would reduce surface leakage was proven. CuBTA on copper surface could prevent Cu oxide from growing, hence it reduced surface leakage current. However, after BTS, the leakage current of CuBTA on copper surface increased. The high temperature would degrade the CuBTA layer as described, hence, Cu oxide would grow on Cu surface, which caused bigger leakage current. The thermal stability of CuBTA also was discussed in this study. CuBTA film would been decomposed at the range of about 150℃ to 200℃. Although the high temperature would degrade the CuBTA layer, the leakage current also was smaller than those without Cu-BTA but oxide passivation.

References

[1] Po-Lin Chen, “Study on Post-Chemical-Mechanical Polishing Cleaning in the Copper Damascene Process”, Master Thesis, Institute of Materials & Mineral Resources Engineering College of Engineering, National Taipei University of Technology, 2001.

[2] G. Raghavan, C. Chiang, P. B. Anders, S. M. Tzeng, R. Villasol, G. Bai, M. Bohr, D. B. Fraser, ” Diffusion of copper through dielectric films under bias temperature stress”, Tjin Solid Films ,pp.168-176, 1995.

[3] J. Noguchi, N. Miura, M. Kubo, T. Tamaru, H. Yamaguchi, N. Hamada, K. Makabe, R. Tsuneda and K. I. Takeda, “Cu-Ion-Migration Phenomena and its Influence on TDDB Lifetime in Cu Metallization”, Annual International Reliability Physics Symposium, IEEE, 2003.

[4] J. M. Steigerwald, S. P. Murarka, R. J. Gutmann, “ Chemical Mechanical Planarization of Microelectronic Materials”, Hohn Wiley & Sons, Inc., 1997.

[5] S. Wolf, “ Silicon Processing For The VLSI ERA”, Lattice Press, California, 1990.

[6] W. A Lanford, P. J. Ding, Wei Wang, S. Hymes, and S.P. Murarka, “ Alloying of copper for use in microelectronic metallization”, Materials Chemistry and Physics, 41, pp.192-198, March 1995.

[7] Z. Stavreva, D. Zeidler, M. Plötner, and K. Drescher, ” Chemical Mechanical Polishing of Copper for Multilevel Metallization”, Applied Surface Science, 91, pp.192-196, 1995.

[8] C. K. Hu and J. M. E. Harper, “ Copper interconnections and reliability ”, Materials Chemistry and Physics. Vol.52, pp.5-16, 1998.

[9] C. Steinbruchel, “ Patterning of copper for multilevel metallization: reactive ion etching and

chemical-mechanical polish", Applied Surface Science, Vol. 91, pp.139-146, 1995.

[10] Hong Xiao, " Introduction to Semiconductor Manufacturing Technology", Prentice-Hall Inc., 2001.

[11] Keng-Ming Liu, "Study on the Chemical Mechanical Polishing of Copper Yhin Films", Masters, Institite of Electronics Engineering, National Chiao-Tung University, 1998.

[12] D. Hymes, H. Li, E. Zhao, and J. D. Larios, "The Challenges of the Copper CMP Clean", Semiconductor International, pp.117-122, June 1998.

[13] V. Nguyen, H. Vankranenburg, P. Woerlee, " Dependency of dishing on polish time and slurry chemistry in Cu CMP", Microelectronic Engineering, 50, pp.403-410, 2000.

[14] Cheng-Ging Chen, "Study on Chemical-Mechanical Polish in the Copper Damascene Process", Master Thesis, Institute of Material Scence and Engineering, National Chiao-Tung University, 2000.

[15] S. L.Cohen, V. A. Brusic, F. B. Kaufman, G. S. Frankel, S. Motake, and B. Rush, "X-Ray Photoelectron Spectroscopy and Ellipsometry Studies of the Electrochemically Controlled Adsorption of Benzontriazole on Copper Surface", Journal of Vaccum Science and Technology, Vol.8, No.3, May/Jun 1990.

[16] N. Elbel, S. Wang, A. Sanger, D. Hadawi, and C. Held, "Copper Post-CMP Brush Cleaning", IEEE IITC, pp.80-82, 1999.

[17] M. S. Tsai, "化學機械研磨後清洗技術簡介", National Nano Device Laboratories, Technology news,Vol. 6, issue 1.

[18] B. E. Douglas, D. H. McDaniel, and J. J. Alezander, " Inorganic Chemistry", John Wiley & Sons, Inc., 1994.

[19] J. H. Chen, C. F. Yeh, J. C. Lin, P. L. Chen, and W. R. Chen, ” The Effect of Metal Chelators on the Post Copper CMP Cleaning of Copper Ions”, Symposium on Nano Device Technology 2000, pp.190-193, May 24-25, 2000.

[20] G. Nanz and L.E. Camiletti, “Modeling of chemical-mechanical polishing A review”, *IEEE*, 1995.

[21] R. Faibish, W. Yoshide, and Y. Cohen, “Contact Angle Study on Polymer-Grafted Silicon Wafers”, Journal of Colloid and Interface Science 256, 341-350, 2002.

[22] S. M. Sze, “Physics of Semiconductor Device”, 2nd edition, John Wiley & Sons, Inc., 1983.

[23] 汪建民, ” 材料分析”, 中國材料科學學會, 2000.

[24] H. Schwenke, J. Knoth, and U. Weisbrod, “Analysis of particles on the surfaces by total reflection X-ray fluorescence spectrometry ”, Particles on Surface 3, Plenum Press, 1991.

[25] W. S. Tait, “An Introduction To Electrochemical Corrosion Testing For Practicing Engineers And Scientists”, Pair O Docs Pubns, 1994.

[26] 李俊義, ” 分析化學”, 科技圖書股份有限公司, 1990.

[27]K. Cho, J. Kishimoto, T. Hashizume, H. W. Pickering, T. Sakurai, “Adsorption and film growth of BTA on the clean and oxygen adsorbed Cu(110) surfaces”, Applied Surface Science, 380-385, 1995.

[28] John C. Vickerman, ” Surface Analysis-The Principal Techniques”, John Wiley & Sons, Inc., 1997.

[29] A. Nishi, M. Sado, T. Miki, Y. Fukui,” Evaluation of the Cu-CMP process by TOF-SIMS and XPS: time dependence of CU surface adsorbents and oxidation states”, Applied Surface Science, 470-472,

2003.

[30] J. Noguchi, N. Ohashi, T. Jimbo, H. Yamaguchi, K. Takeda, K. Hinode,” Effect of NH_3-Plasma Treatment and CMP Modification on TDDB Improvement in Cu Metallization” , IEEE Transaction on Electron Device, VOL. 48, NO. 7, 2001.

Table.1-1 Properties of low resistivity metals

	Ag	**Al**	**Al Alloy**	**Au**	**Cu**	**W**
Resistivity(μΩ-cm)	1.59	2.66	~3.5	2.35	1.67	5.65
Electromigration Resistance (at 0.5μm)	Poor	Poor	Fair-Poor	Very Good	Good	Very Good
Corrosion Resistance	Poor	Good	Good	Excel	Poor	Good
Adhesion to SiO_2	Poor	Good	Good	Poor	Poor	Poor
Si Deep Levels	Yes	NO	NO	YES	YES	NO
CVD Processing	None	?	None	None	Avail	Avail
RIE Etch	None	Avail	Avail	None	?	Avail

Table.2-1 Three types of chelator solutions

Type	**Trade name**	**Typical structure**
1	Citric acid	$OOCCH_2C(OH)(COOH)CH_2COOH$
	ADPA-60	$CH_3C(OH)(PO_3H_2)_2$
2	EDTA	$NaOOCCH_2)_2NCH_2CH_2N(CH_2COONa)_2$
	422-25S	$(CH_2PO_3H_2)_2N(CH_2)_2N(CH_2PO_3H_2)_2$
3	Catechol	$C_6H_6O_2$
	TBC	$C_{10}H_{14}O_2$

Table.2-2 The cleaning steps and parameters of SSEC-M50

SSEC-M50		**Cleaning time**	**Flow rate**	**Rotation rate of water**
Step1	Chelator cleaning	Parameter (15 cycles/min)	150 ml/min	800 rpm
Step2	DIW rinse	7 cycle (15 cycles/min)	unknown	800 rpm
Step3	Dry spin	25 sec	off	2500 rpm

Table.2-3 Polishing parameters for cleaning experiment.

IPEC 372M	**Phase1**	**Phase2**
Down force	5.0 psi	2.0 psi
Back pressure	1.5 psi	0 psi
Platen/carrier speed	42/45 rpm	20/25 rpm
Slurry flow rate	150 ml/min	150 ml/min
Polishing Time	60 sec	20 sec
Temperature	27 ℃	27 ℃
Polishing Pad	Rodel Politex Regular E.™	
Carrier Film	Rodel R200 T3	
Slurry formulation	30wt.% SS-25	DIW rinse

Table.2-4 The results of contact angle in the wetting ability experiment.

Type	Trade name	Contact angle
1	Citric acid	37.2℃
	ADPA-60	38.4℃
2	EDTA	36.1℃
	422-25S	34.8℃
3	Catechol	41.2℃
	TBC	43.5℃

Table.3-1 Polishing parameters for surface morphology evaluation.

IPEC 372M	***1st step***	***2nd step***	
		KOH buffing	***HNO$_3$/BTA buffing***
Down force	5.0 psi	2.0 psi	2.0 psi
Back pressure	1.5psi	0 psi	0 psi
Platen/carrier speed	42/45 rpm	20/25 rpm	20/25 rpm
Slurry flow rate	150 ml/min	150 ml/min	150 ml/min
Temperature	27 ℃	27 ℃	27 ℃
Polishing Pad	Rodel Politex Regular E.™		
Carrier Film	Rodel R200 T3		
Slurry formulation	**10% 100S** + 10% H_2O_2	KOH	***HNO$_3$/BTA=0.6/1E^{-3}M***
Polish time	1min	parameter	1min

Table.3-2 Polishing parameters of evaluating passivation effect on surface leakage.

IPEC 372M	**Phase1** **Cu removing**	**Phase2** **Ta removing**	**Buffing**
Down force	**5.0 psi**	**5.0 psi**	**2.0 psi**
Back pressure	**1.5 psi**	**1.5 psi**	**0 psi**
Platen/carrier speed	**42/45 rpm**	**42/45 rpm**	**20/25 rpm**
Slurry flow rate	**150 ml/min**	**150 ml/min**	**150 ml/min**
Polishing Time	**160 sec**	**180 sec**	**180 sec**
Temperature	**27 ℃**	**27 ℃**	**27 ℃**
Polishing Pad	**Rodel IC 1400™**	**Rodel Politex Regular E.™**	
Carrier Film	**Rodel R200 T3**		
Slurry formulation	**10% 100S** **+ 10% H_2O_2**	**10% 50ck** **+ 10% H_2O_2**	**HNO_3/BTA** **=0.6/1E^{-3}M** **or 1M KOH**

Table.3-3 The cleaning steps and parameters of SSEC-M50

SSEC-M50		***Cleaning time***	***Flow rate***	***Rotation rate of water***
Step1	Citric acid cleaning	15 cycles (15 cycles/min)	150 ml/min	800 rpm
Step2	DIW rinse	7 cycles (15 cycles/min)	unknown	800 rpm
Step3	Dry spin	25 sec	off	2500 rpm

Table.3-4 The result of contact angle after immersing of chelator solutions. The concentration of chelator solutions were 0.2M.

The Conditions of Cu Film	The Result of Contact angle
Pure Cu Film	48.5°
CuBTA on The Cu Film	88.1°
CuBTA on The Cu Film with immersing of Citric Acid	53°
CuBTA on The Cu Film with immersing of ADPA-60	86.2°
CuBTA on The Cu Film with immersing of EDTA	85.8°
CuBTA on The Cu Film with immersing of 422-25S	86.3°
CuBTA on The Cu Film with immersing of Catechol	74.7°
CuBTA on The Cu Film with immersing of TBC	77.7°

Table.3-5 The result of contact angle after immersing of modified citric acid.

The Conditions of Cu Film	**The Result of Contact angle**
CuBTA on The Cu Film with immersing of 0.2M Citric Acid (pH=1.7)	**53°**
CuBTA on The Cu Film with immersing of 0.2M Citric Acid (pH=8.7)	**71.4°**
CuBTA on The Cu Film with immersing of 1E-3M Citric Acid (pH=3.2)	**68°**
CuBTA on The Cu Film with immersing of 1E-3M Citric Acid (pH=8.7)	**85.6°**

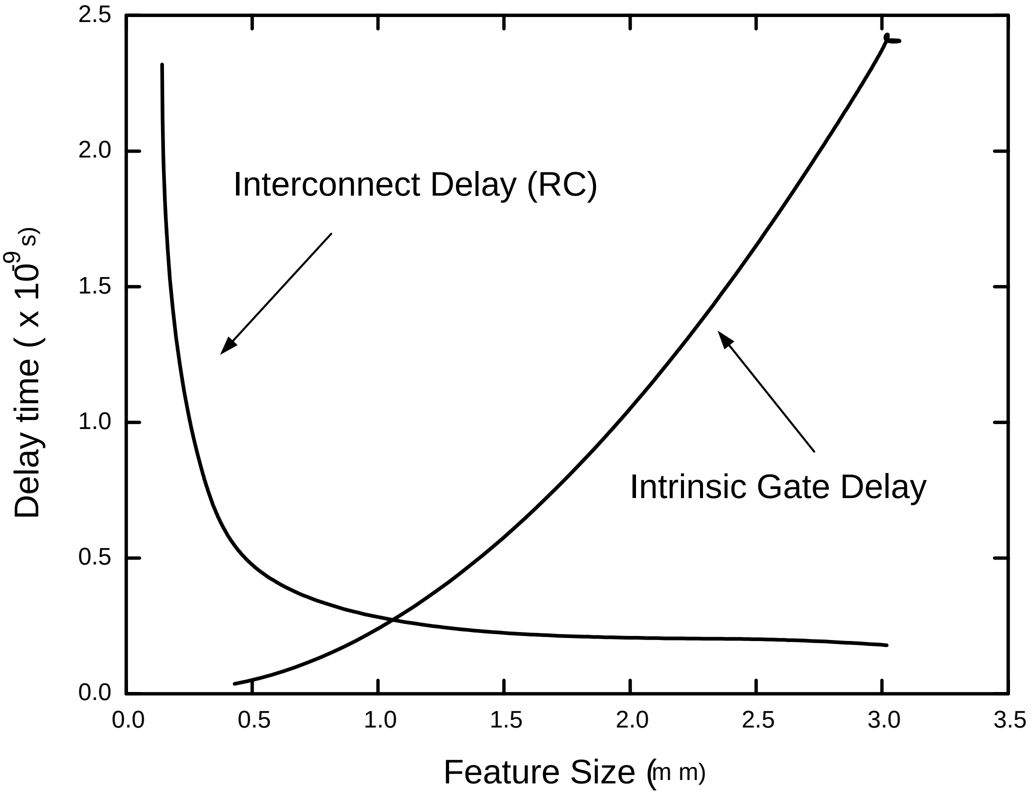

Figure.1-1 Comparison of intrinsic gate delay and interconnect delay (RC) as a function of feature size.

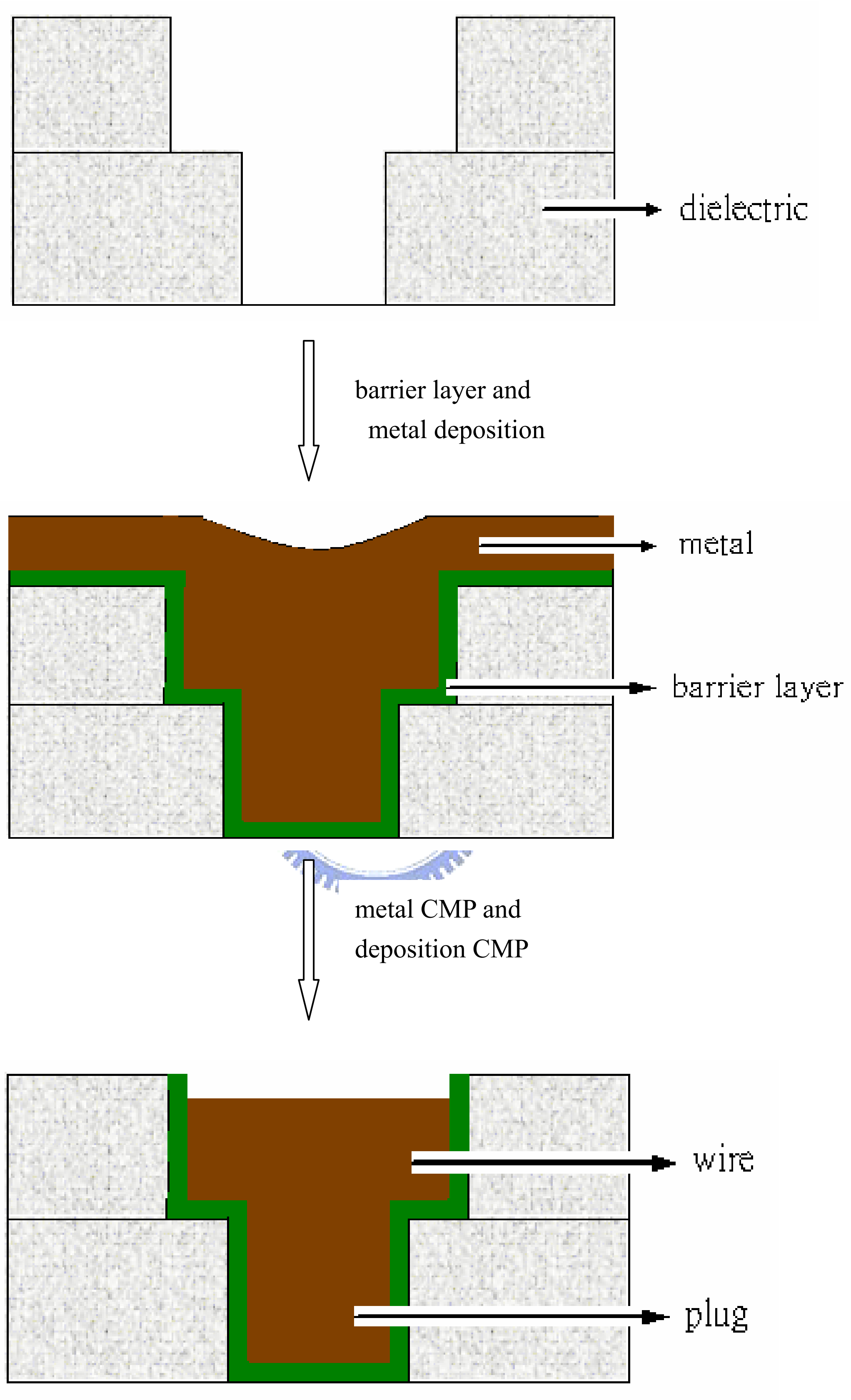

Figure.1-2 Dual damascene process.

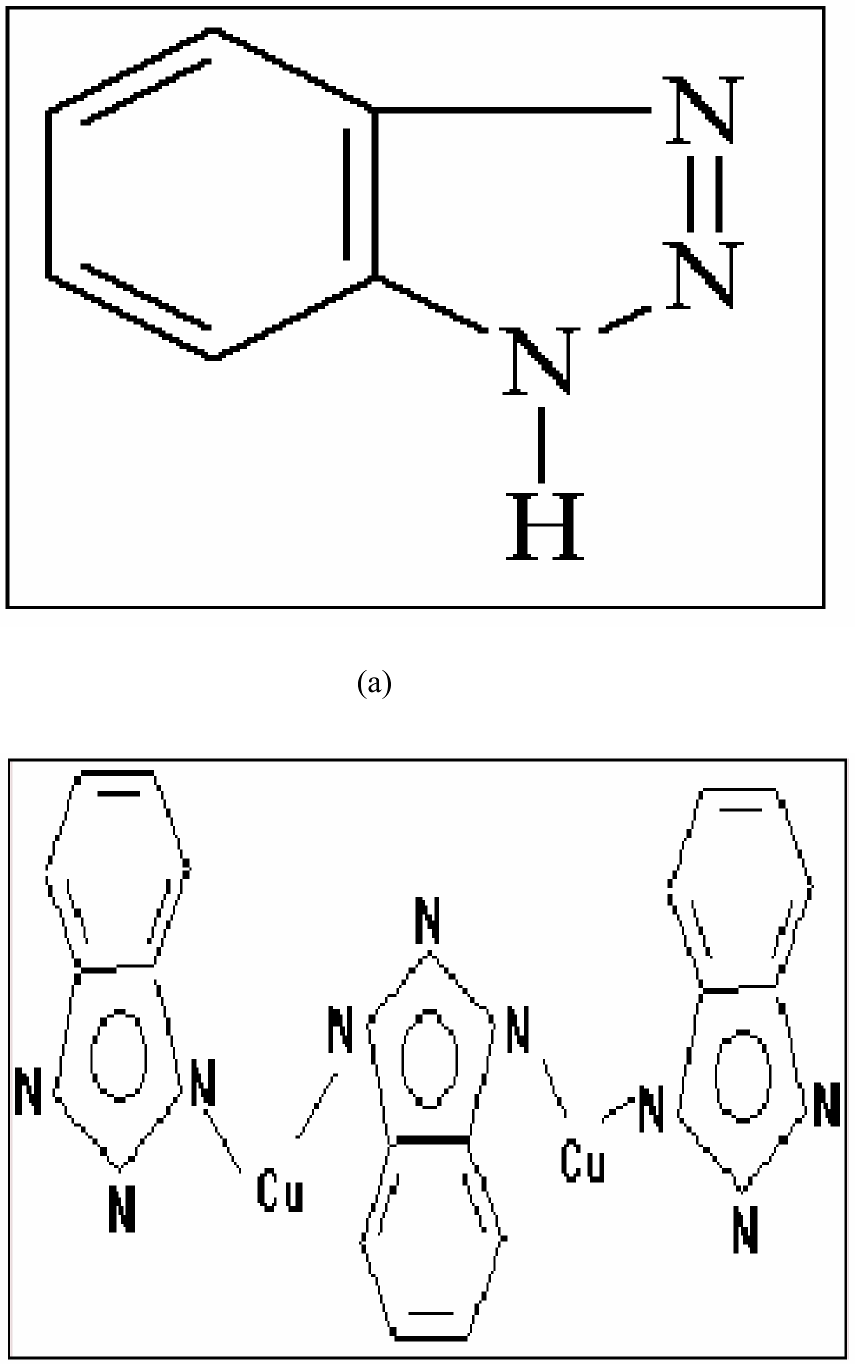

(a)

(b)

Figure.1-3 (a) 1H-BTA structure (b) Cu(Ⅰ)-BTA structure.

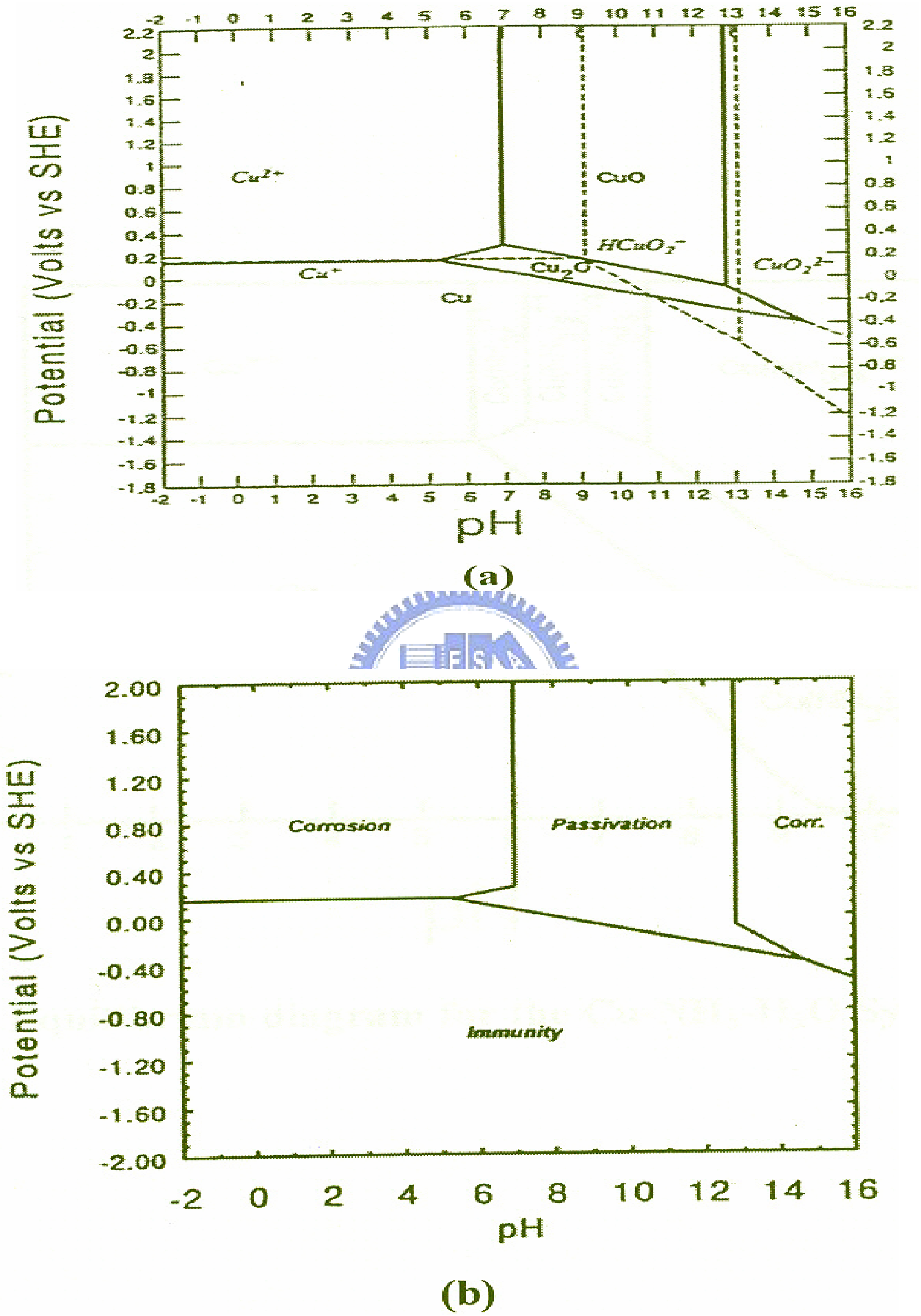

Figure.1-4 (a) Pourbaix diagram for the Cu-H_2O system. (b) Regions of corrosion, passivation, and immunity.

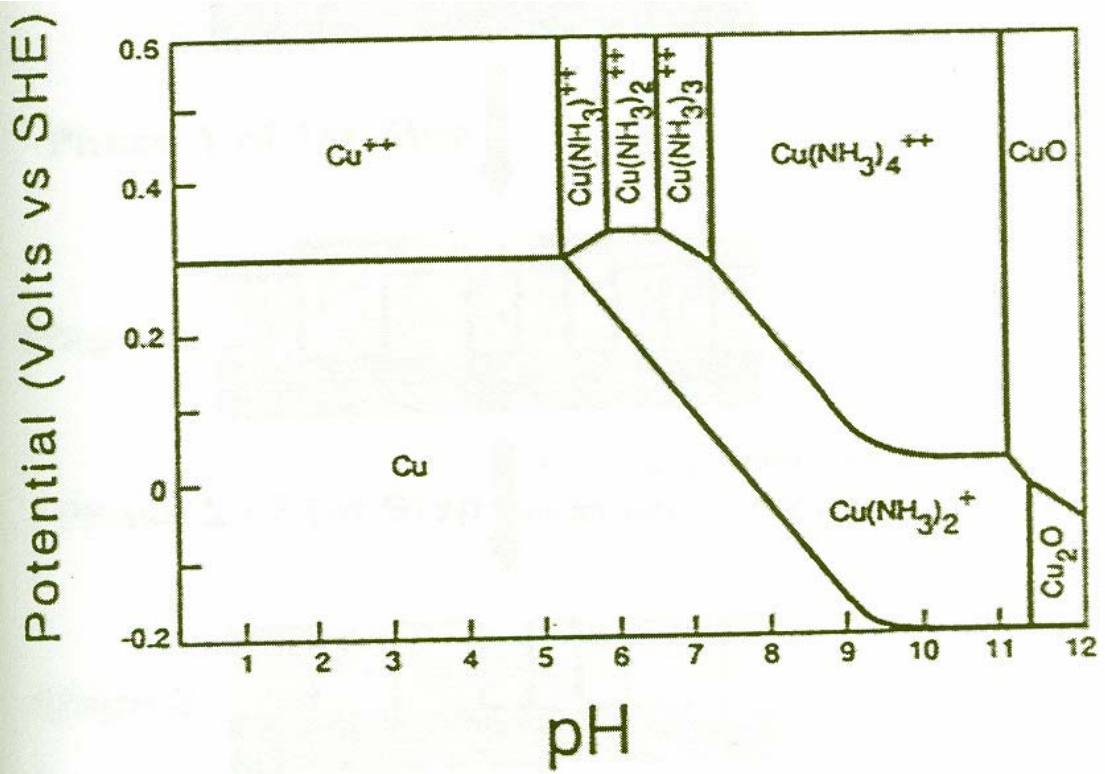

Figure.1-5 Equilibrium diagram for the Cu-NH3-H_2O system.

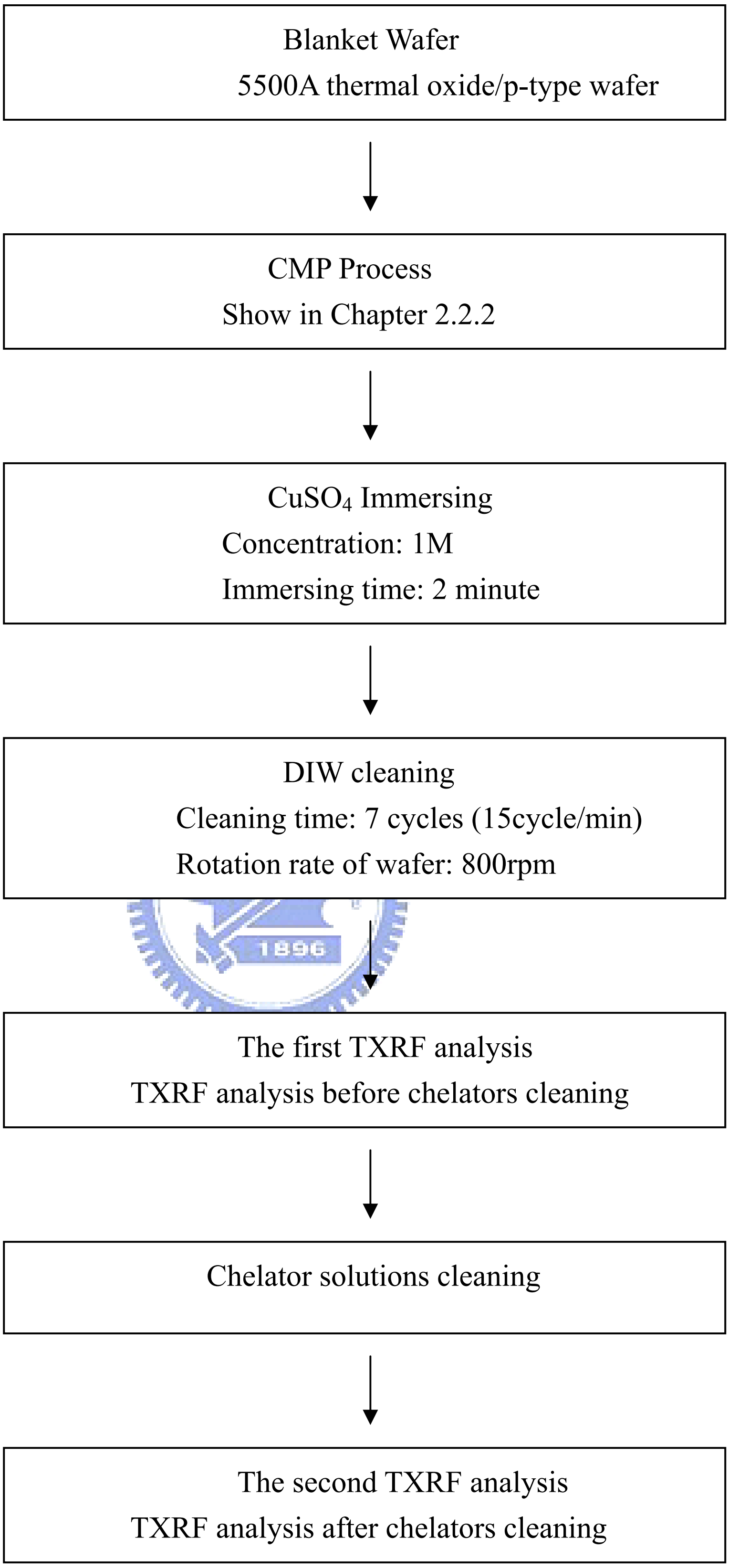

Figure.2-1 The cleaning experiment flow

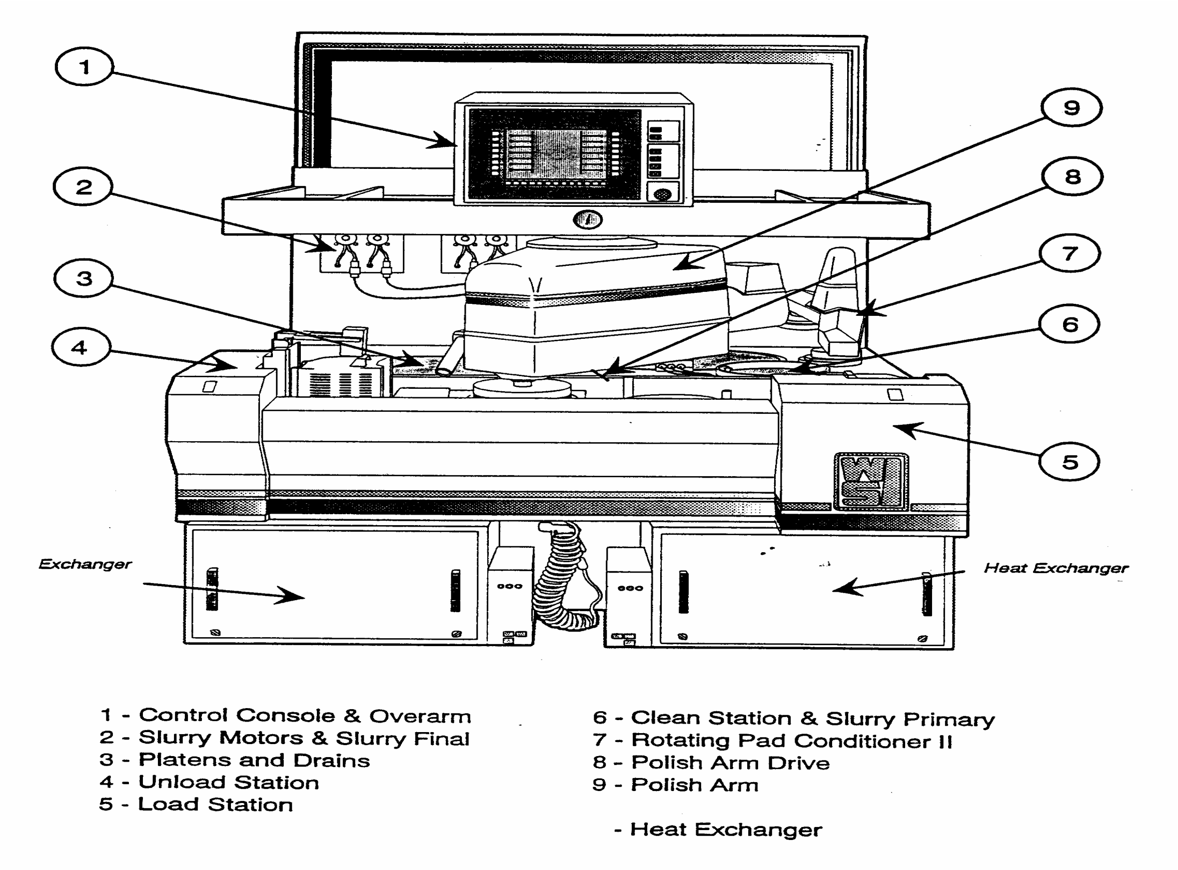

(a)

Figure.2-2 (a) Schematic diagram of the Westech Model 327M CMP polisher

(b) Platen assemblies of the Westech Model 327M CMP polisher.

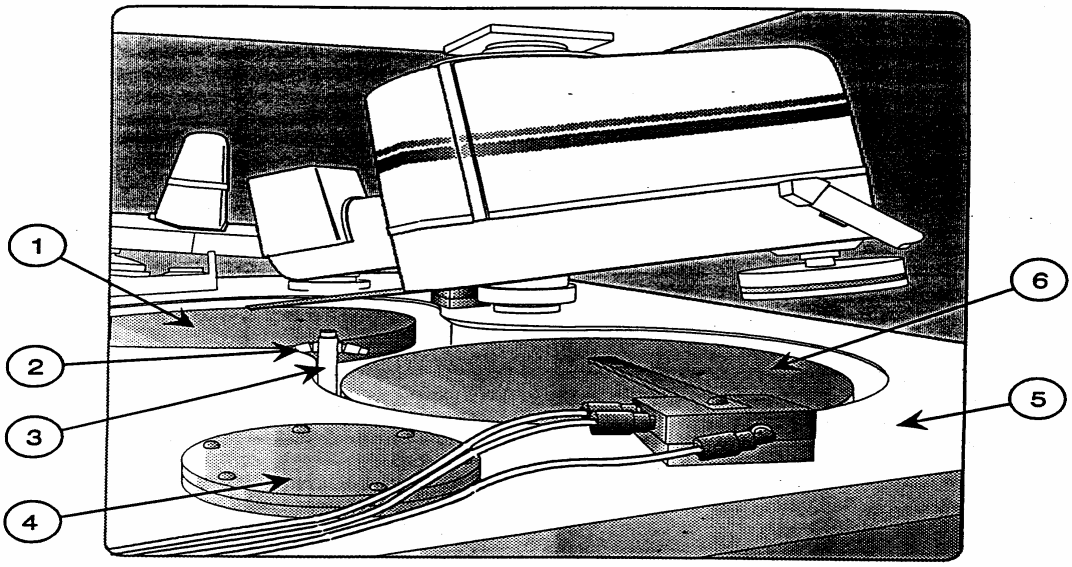

1 - Primary Platen, Cooled (372-21110)
2 - Spray Nozzle (372M-44160)
3 - Spray Tube (372M-44160)
4 - Pad Conditioner Cover (372M-44160)
5 - Contour Top (372M-44160)
6 - Final Platen, Cooled (372-21111)

Figure.2-2 (a) Schematic diagram of the Westech Model 327M CMP polisher
(b) Platen assemblies of the Westech Model 327M CMP polisher.

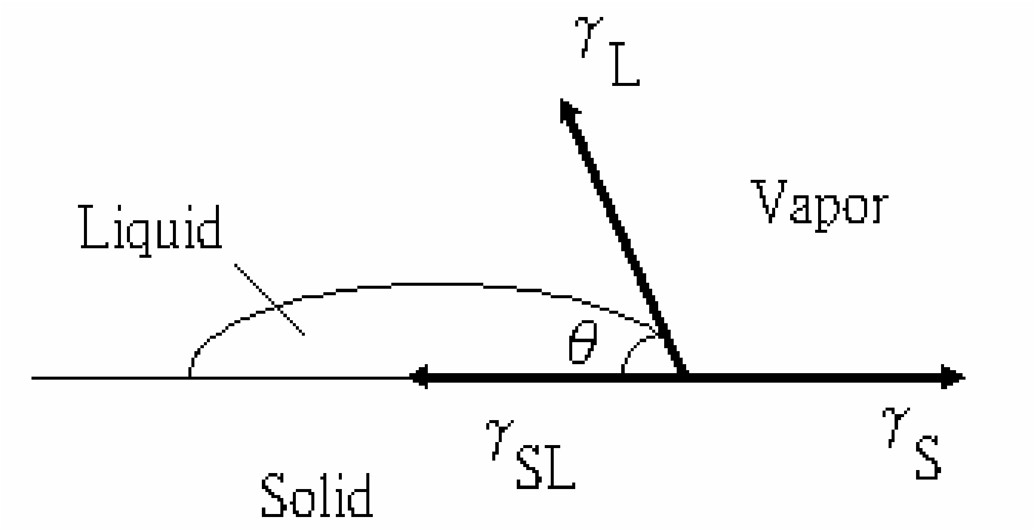

Figure.2-3 Diagram of a liquid drop showing the contact angle.

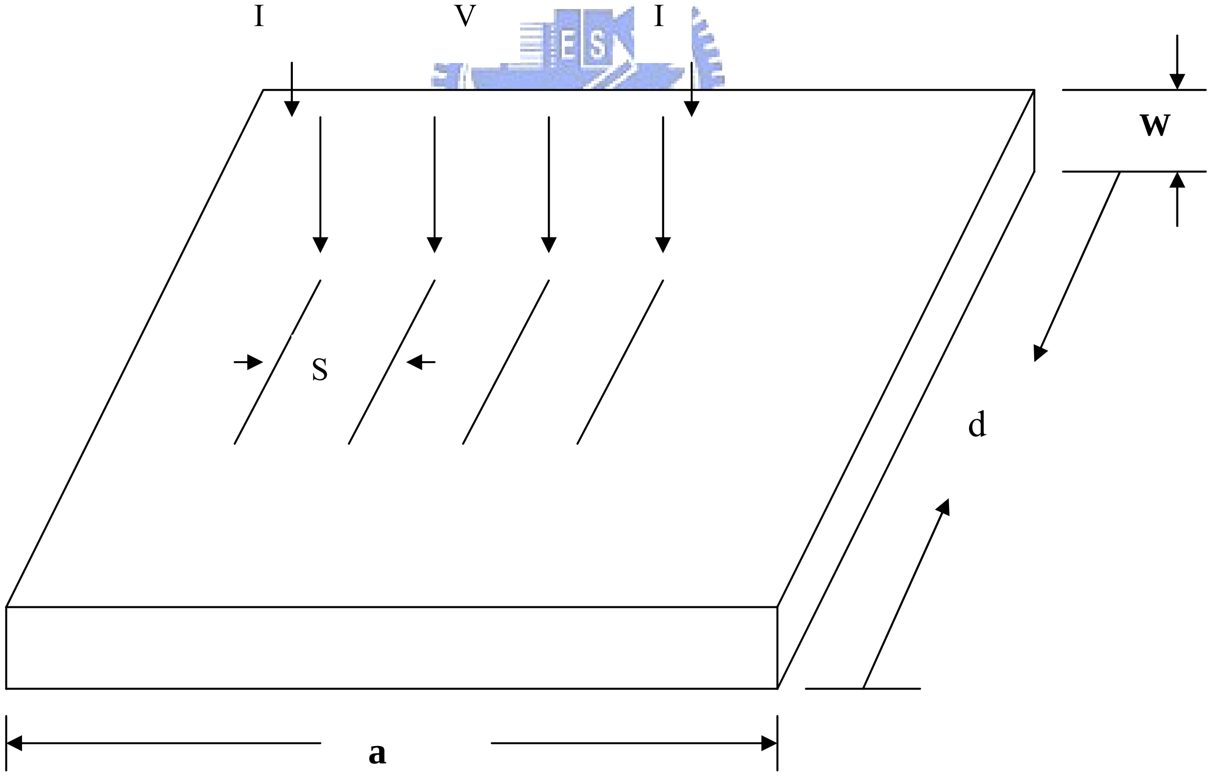

Figure.2-4 Arrangement for four points measurement.

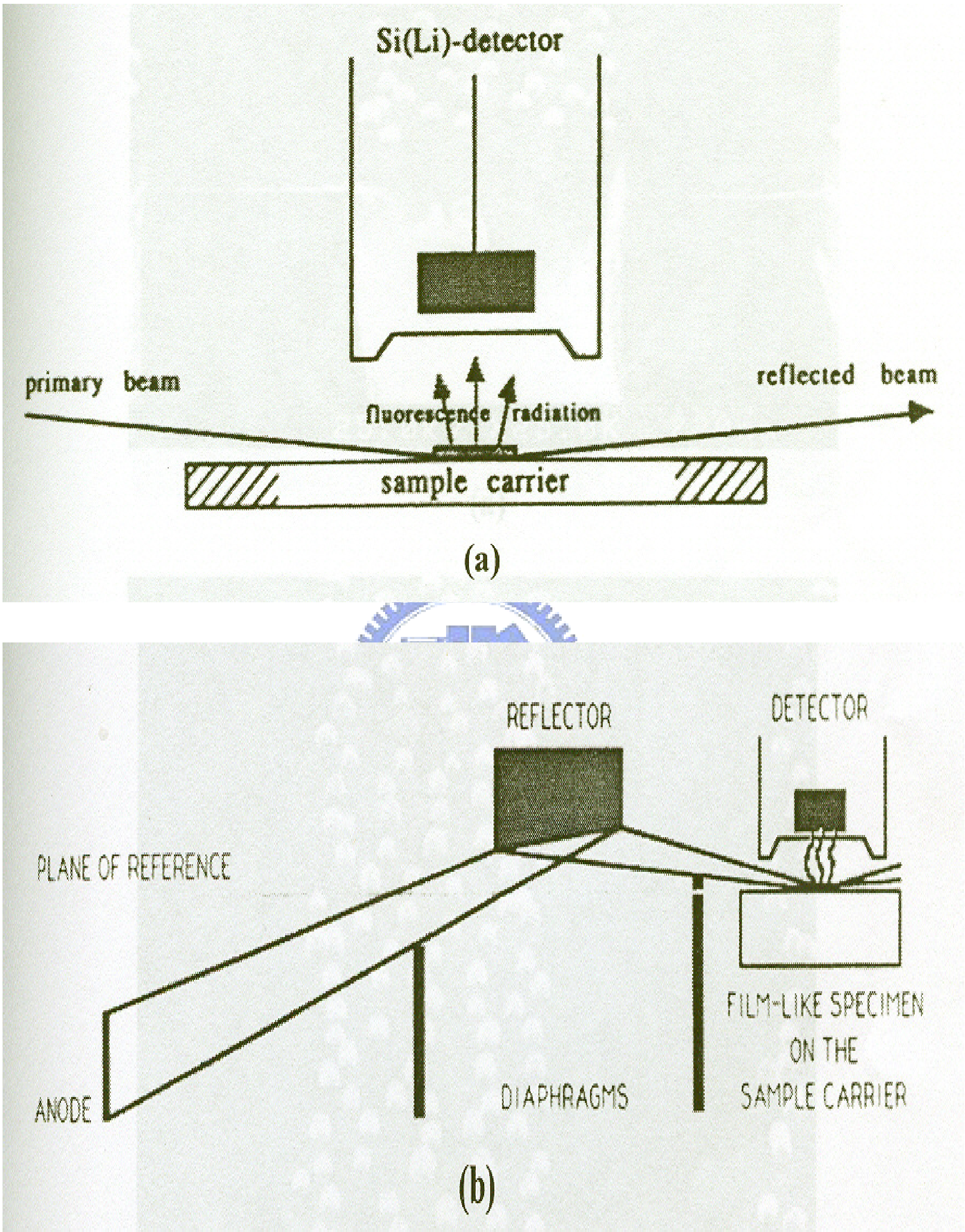

Figure.2-5 (a) Arrangement for TXRF analysis (b) Path of the X-rays in a commercially available TXRF instrument.

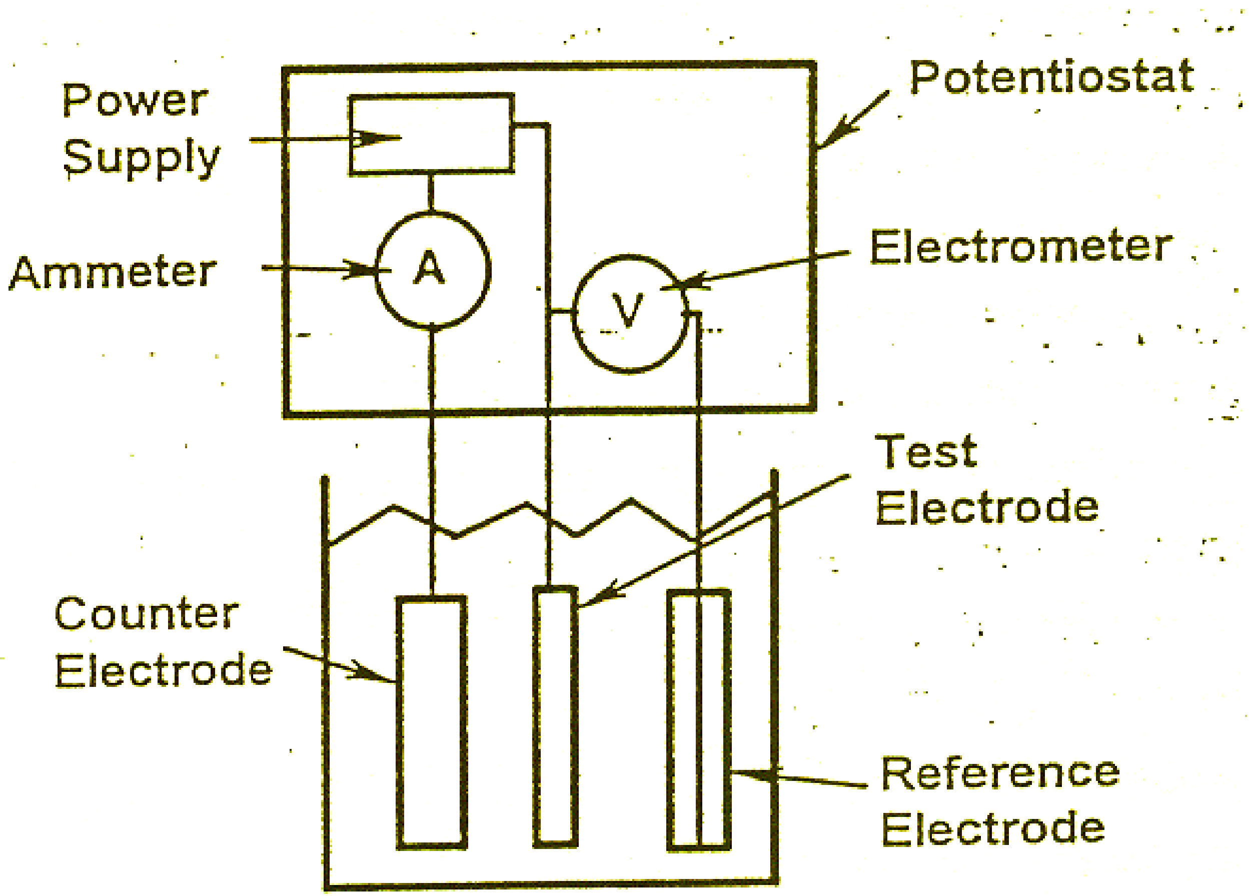

Figure.2-6 Three electrode test cell schematic.

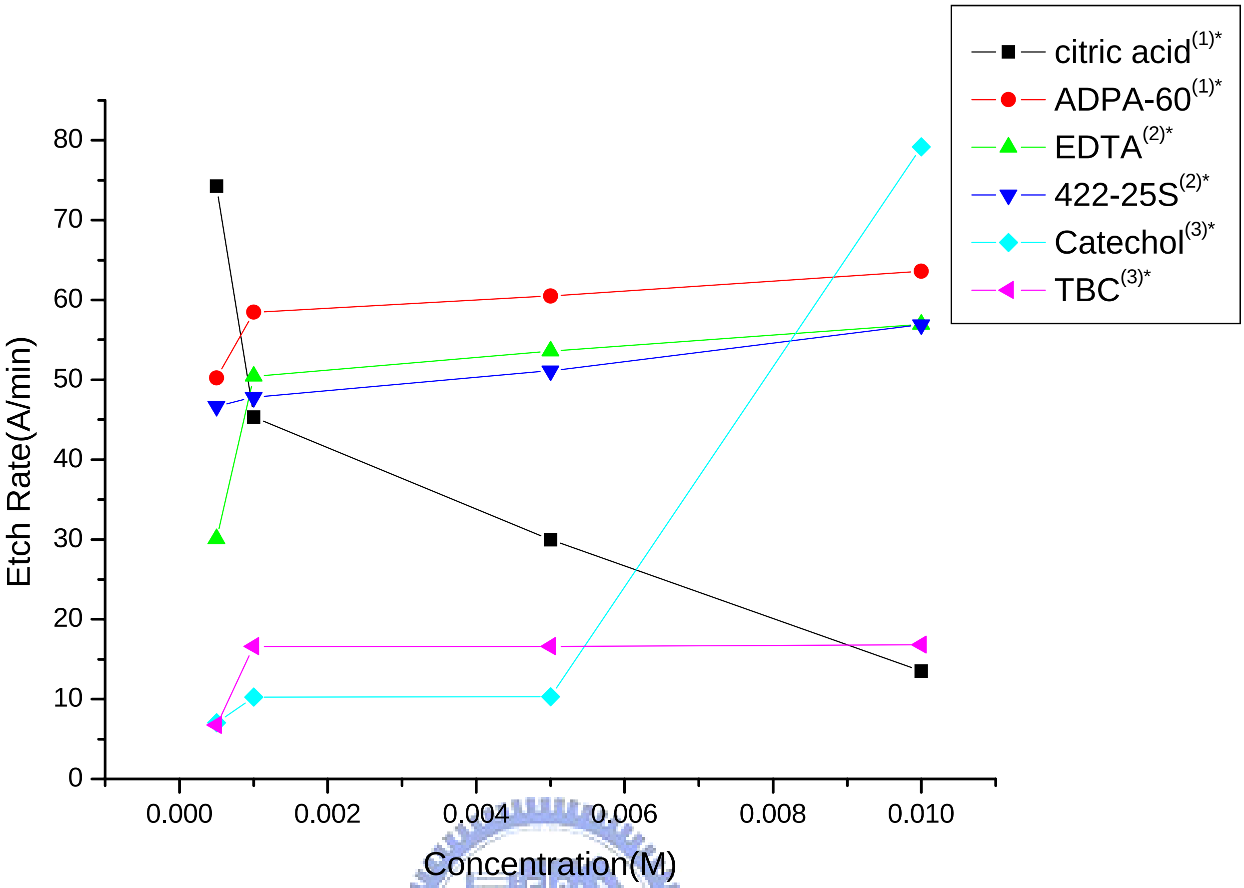

Figure.2-7 The corrosion effect of chelator solutions copper films.
*refer to the type of chelators.

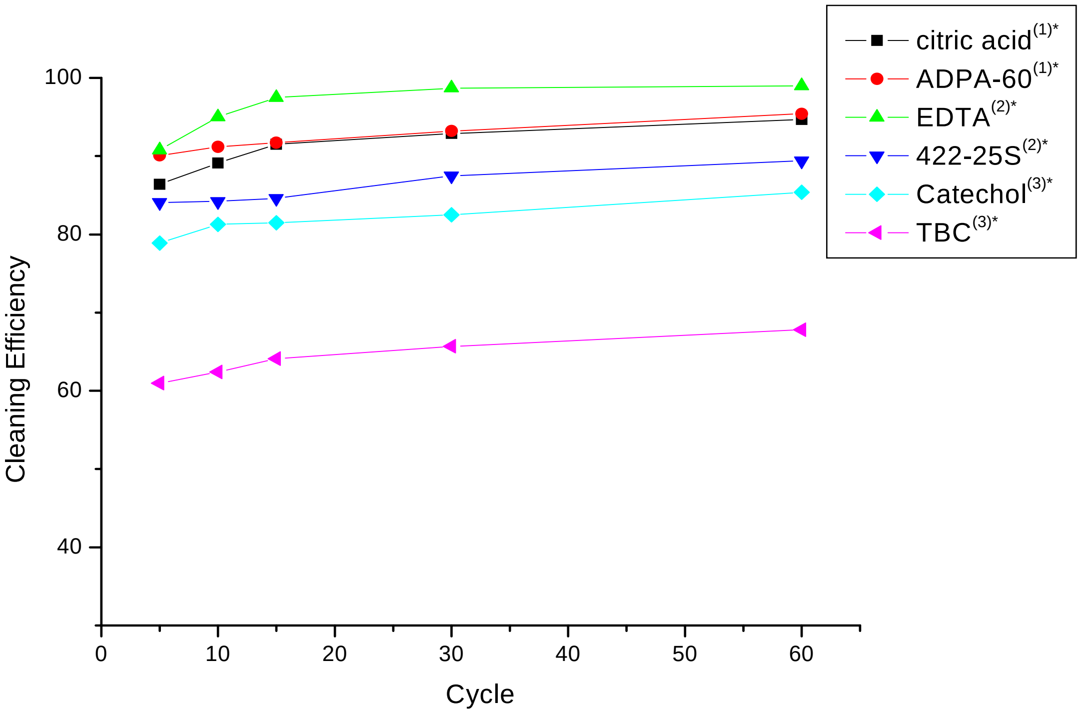

Figure.2-8 The cleaning efficiency as a function of cycle with concentration=5E^{-4}M. *refer to the type of chelators.

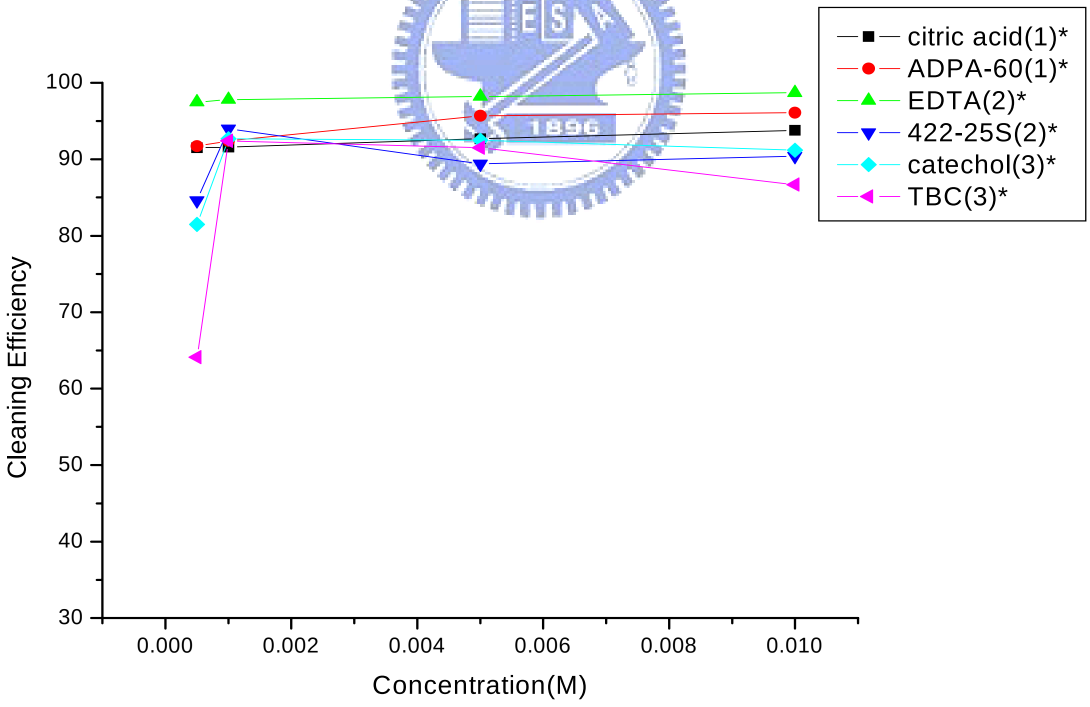

Figure.2-9 The cleaning efficiency as a function of concentration with cleaning cycle=15. *refer to the type of chelators.

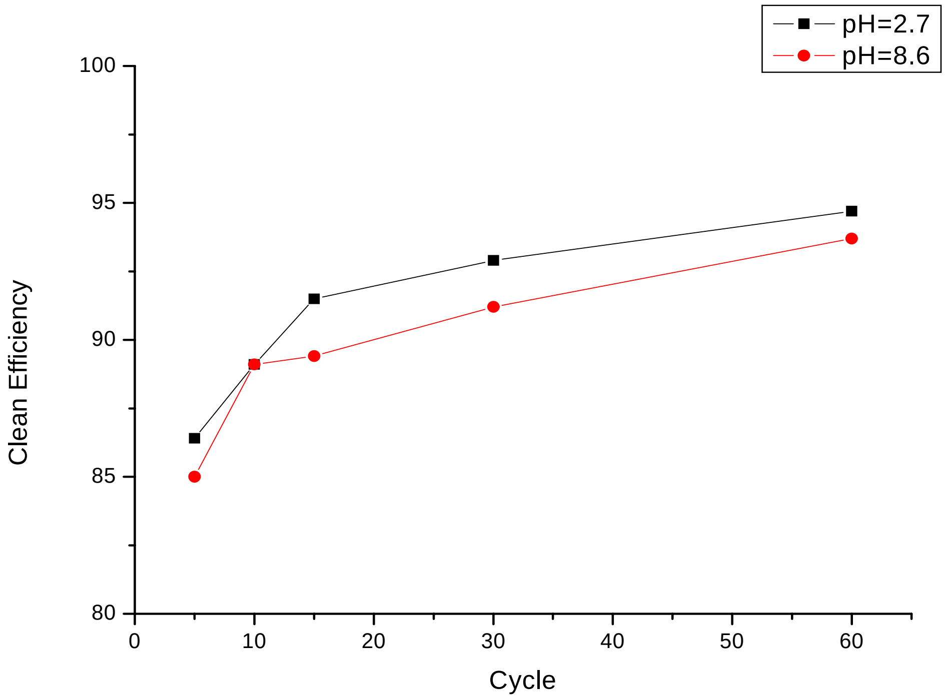

Figure.2-10 The cleaning efficiency as a function of citric acid cleaning cycle with concentration=$5E^{-4}$M.

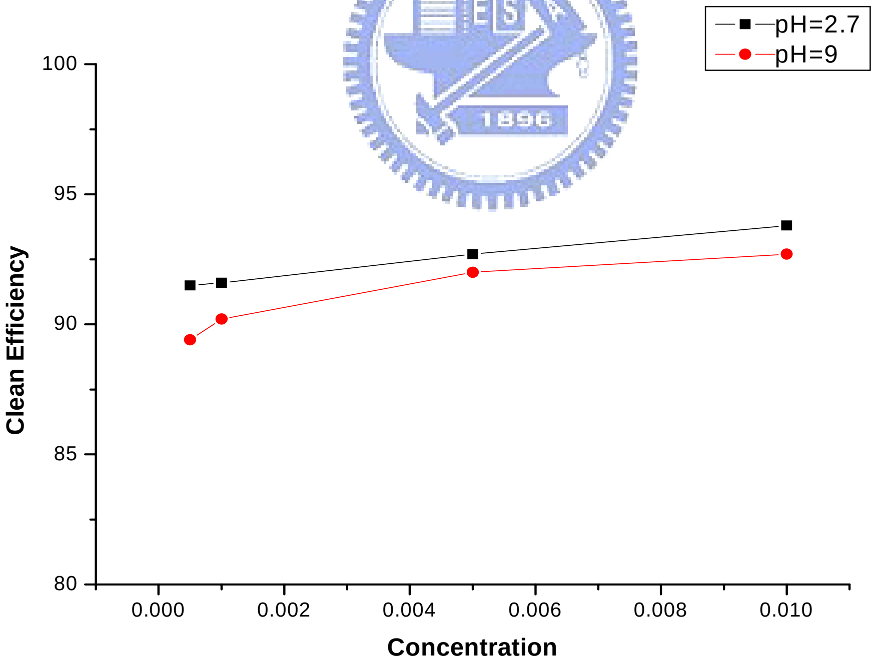

Figure.2-11 The cleaning efficiency as a function of citric acid concentration with cleaning cycle=15.

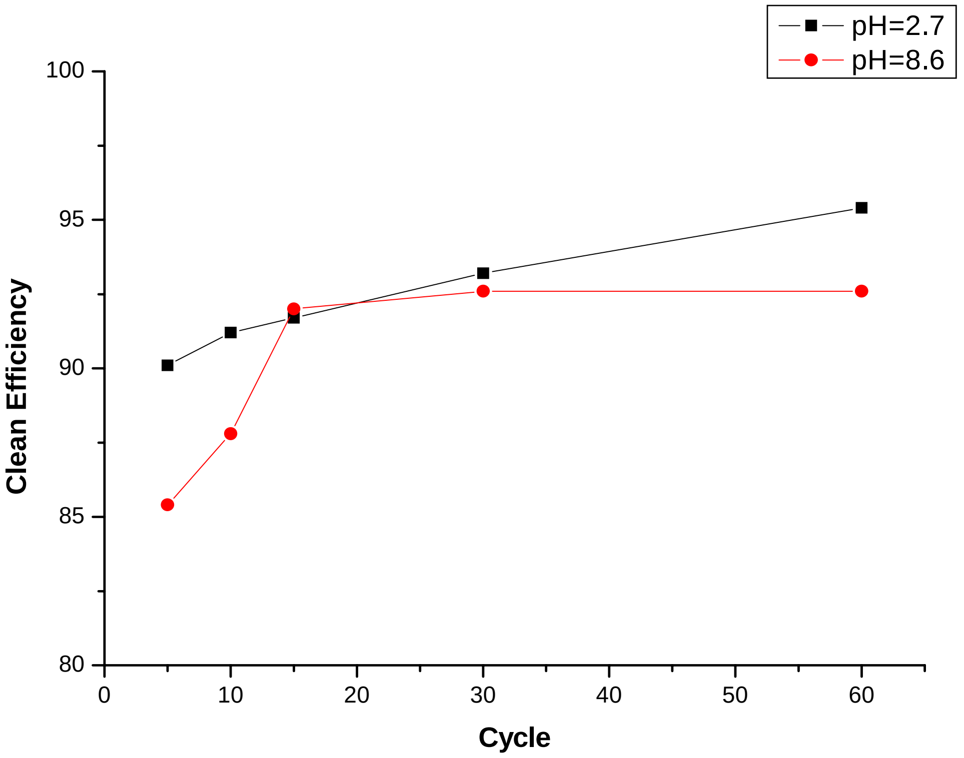

Figure2-12 The cleaning efficiency as a function of ADPA-60 cleaning cycle with concentration=5E^{-4}M.

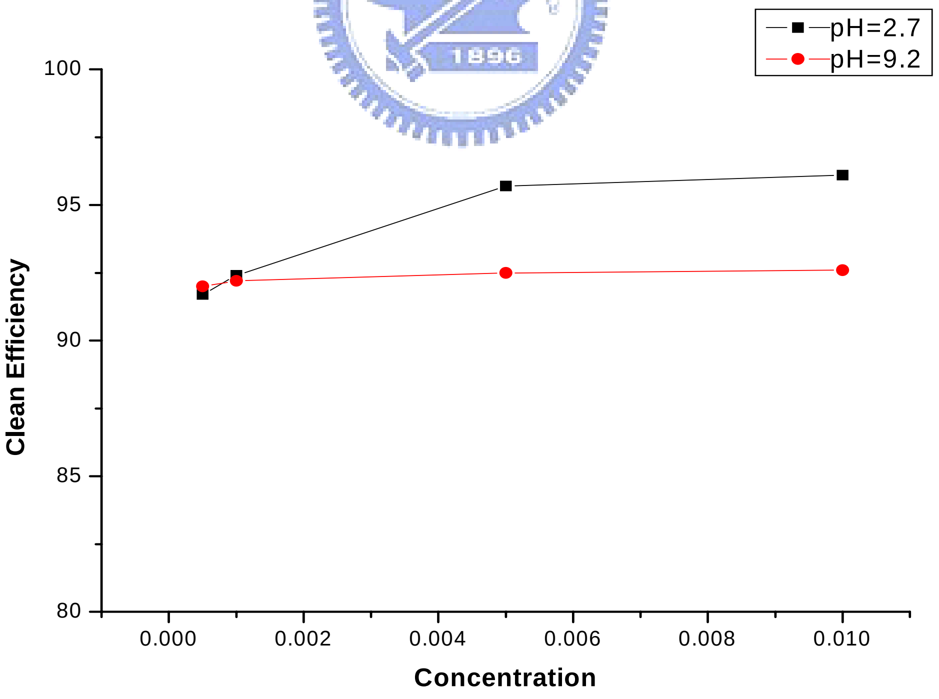

Figure.2-13 The leaning efficiency as a function of ADPA-60 oncentration with cleaning cycle=15.

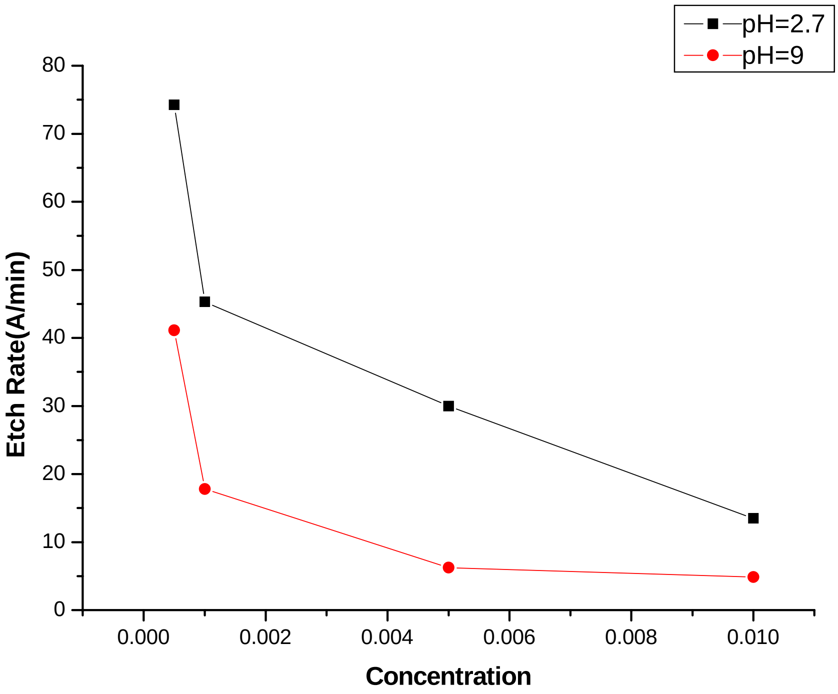

Figure.2-14 The etch rate as a function of citric acid concentration at different pH.

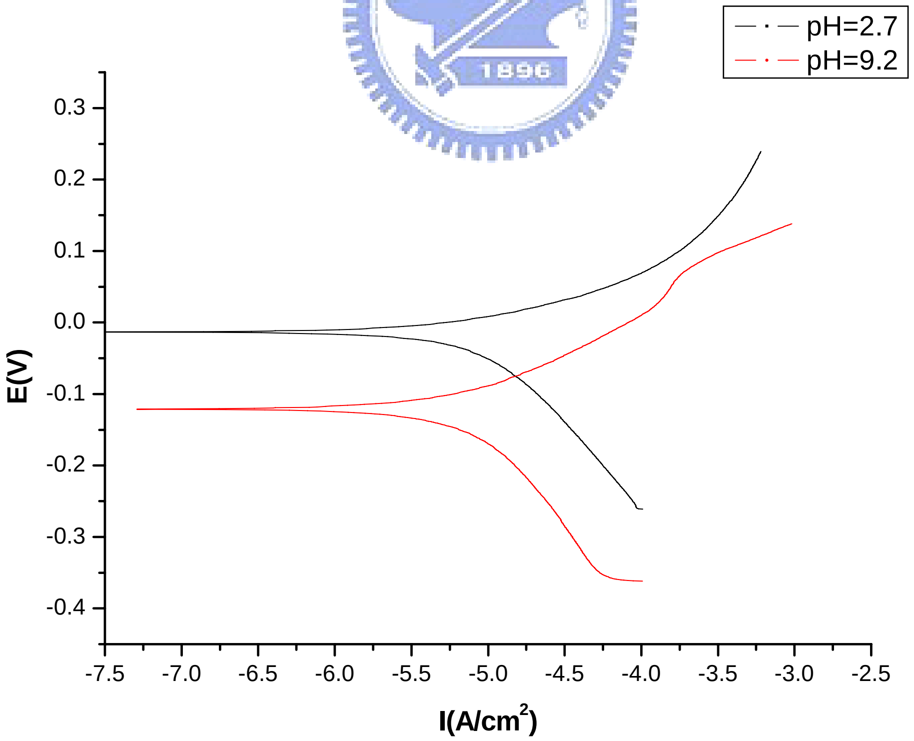

Figure.2-15 Tafel diagram of citric acid with different pH.

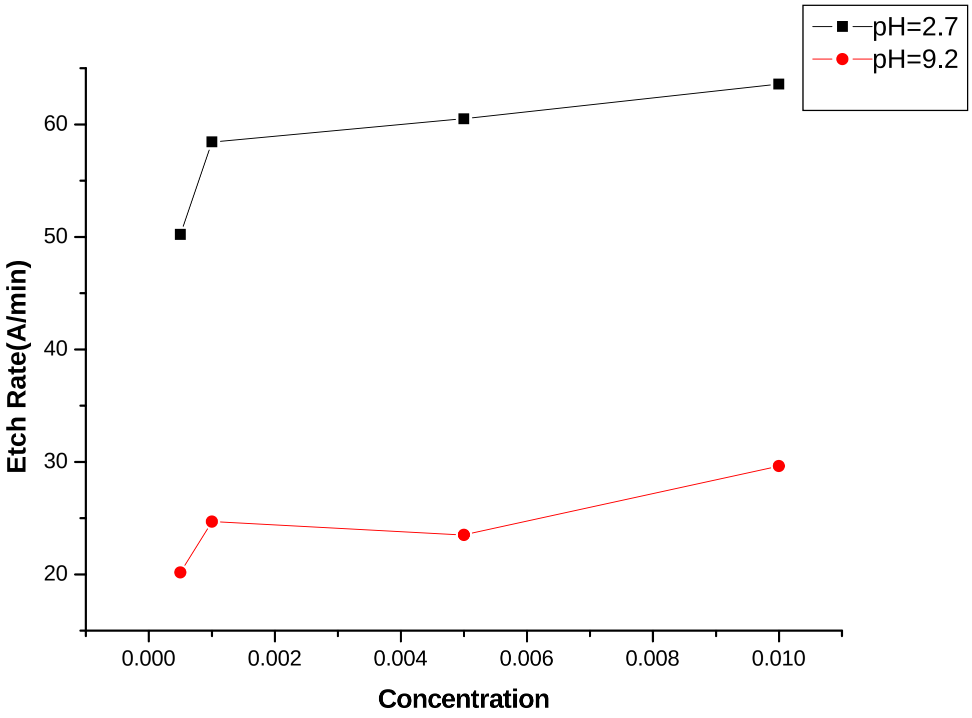

Figure.2-16 The etch rate as a function of ADPA-60 concentration at different pH.

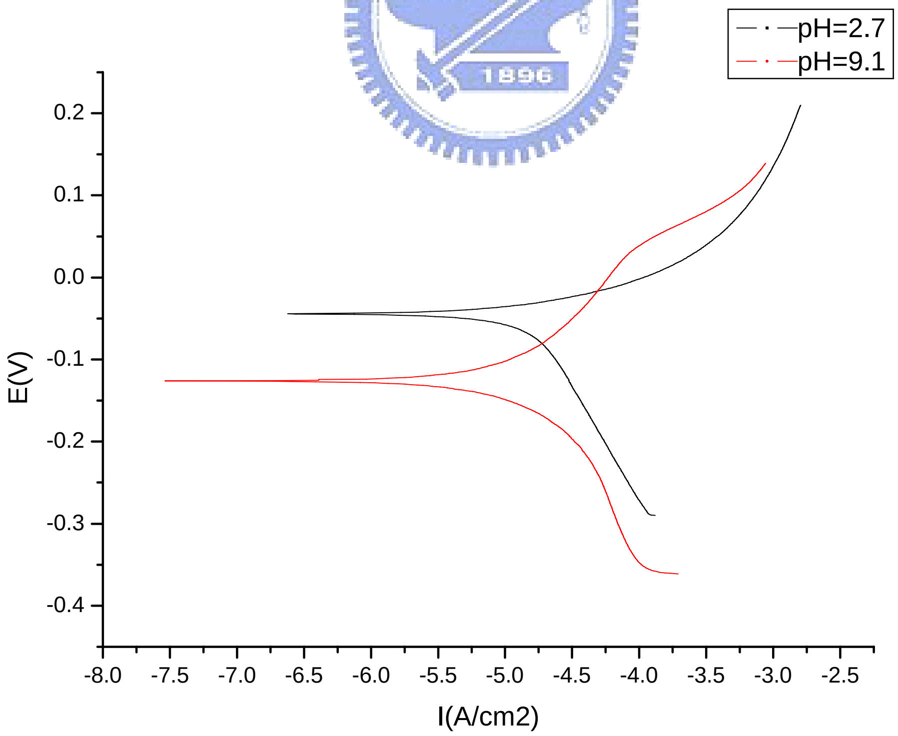

Figure.2-17 Tafel diagram of ADPA-60 with different pH.

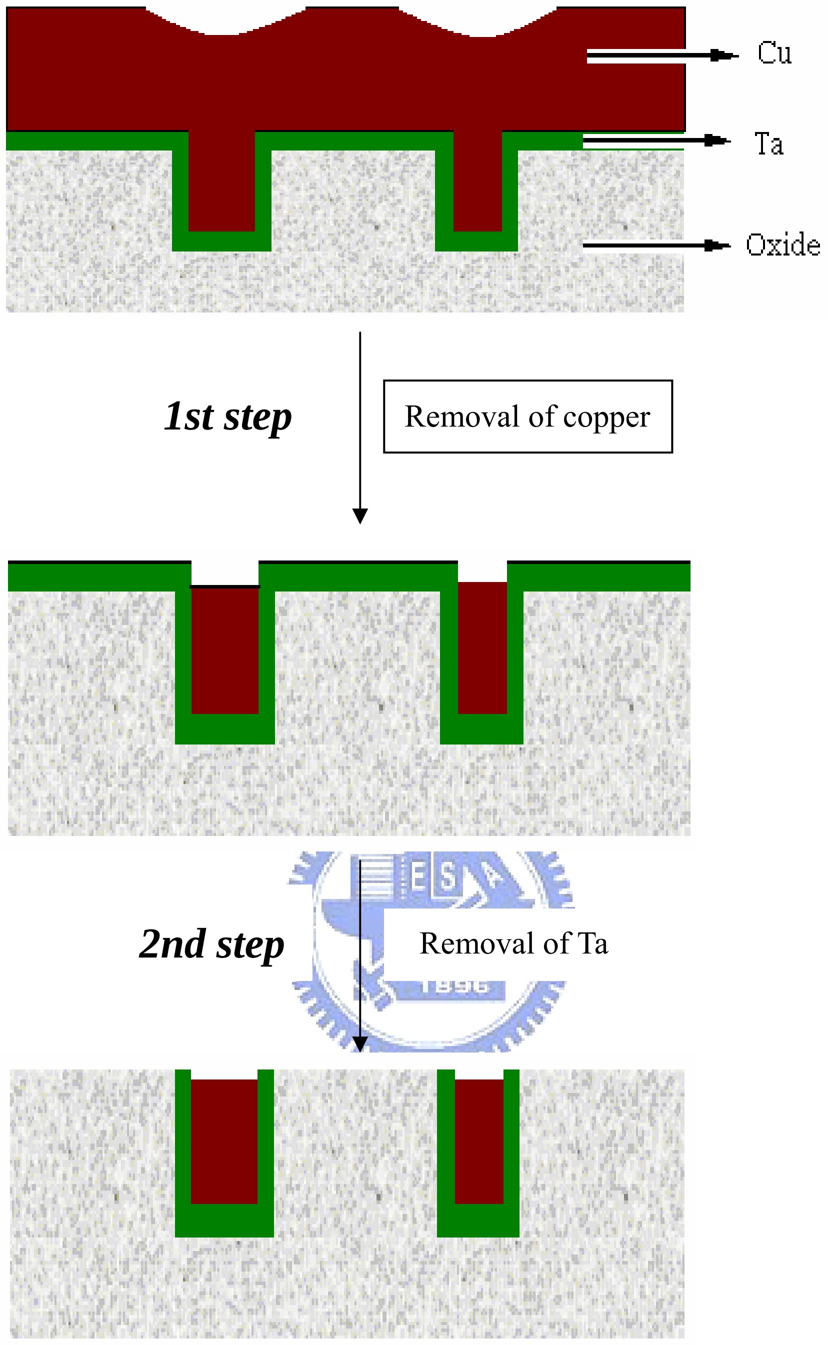

Figure.3-1 The scheme of the two-steps CMP in the damascene process.

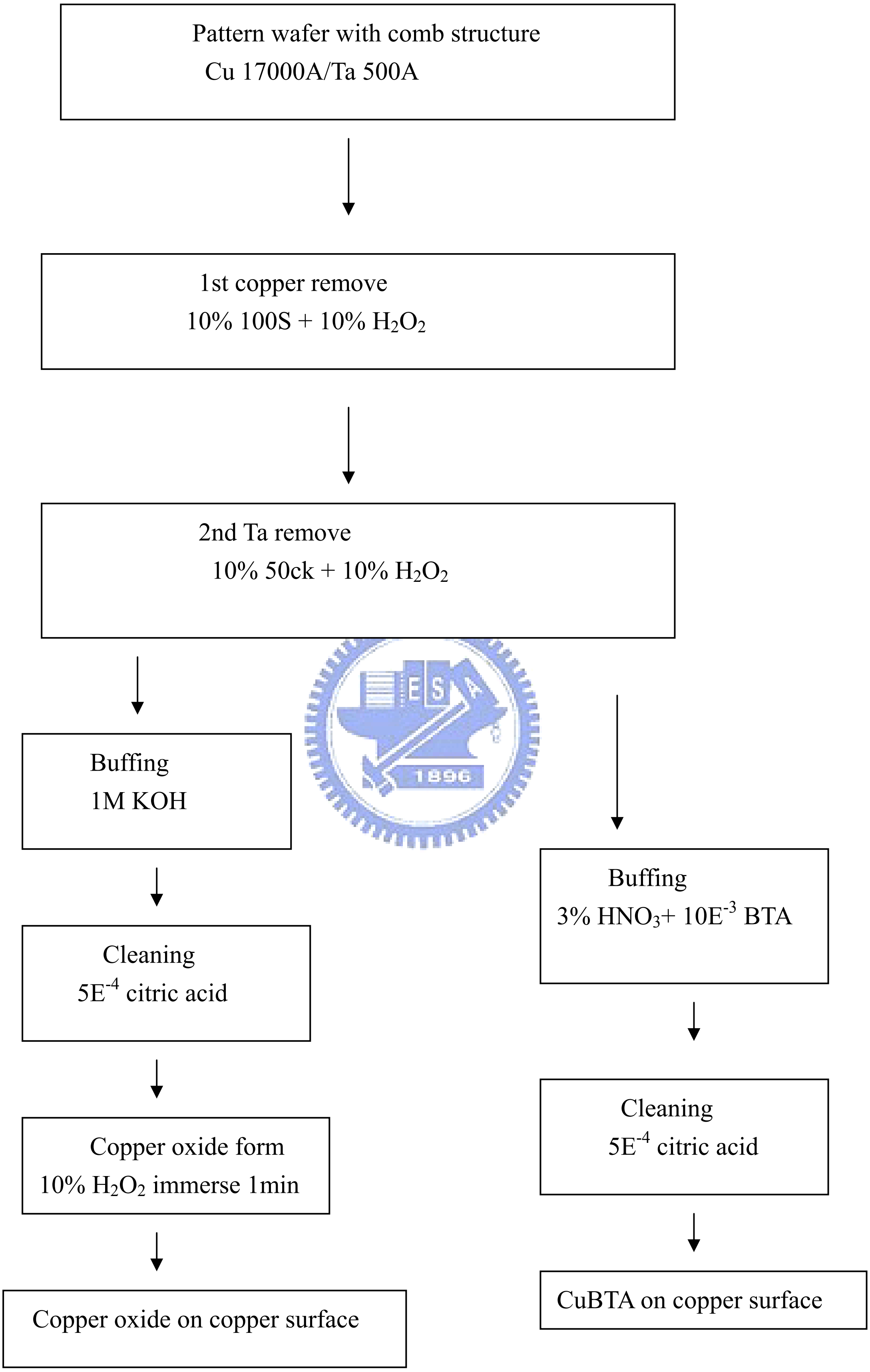

Figure.3-2 Experiment flow of evaluating passivation effect.

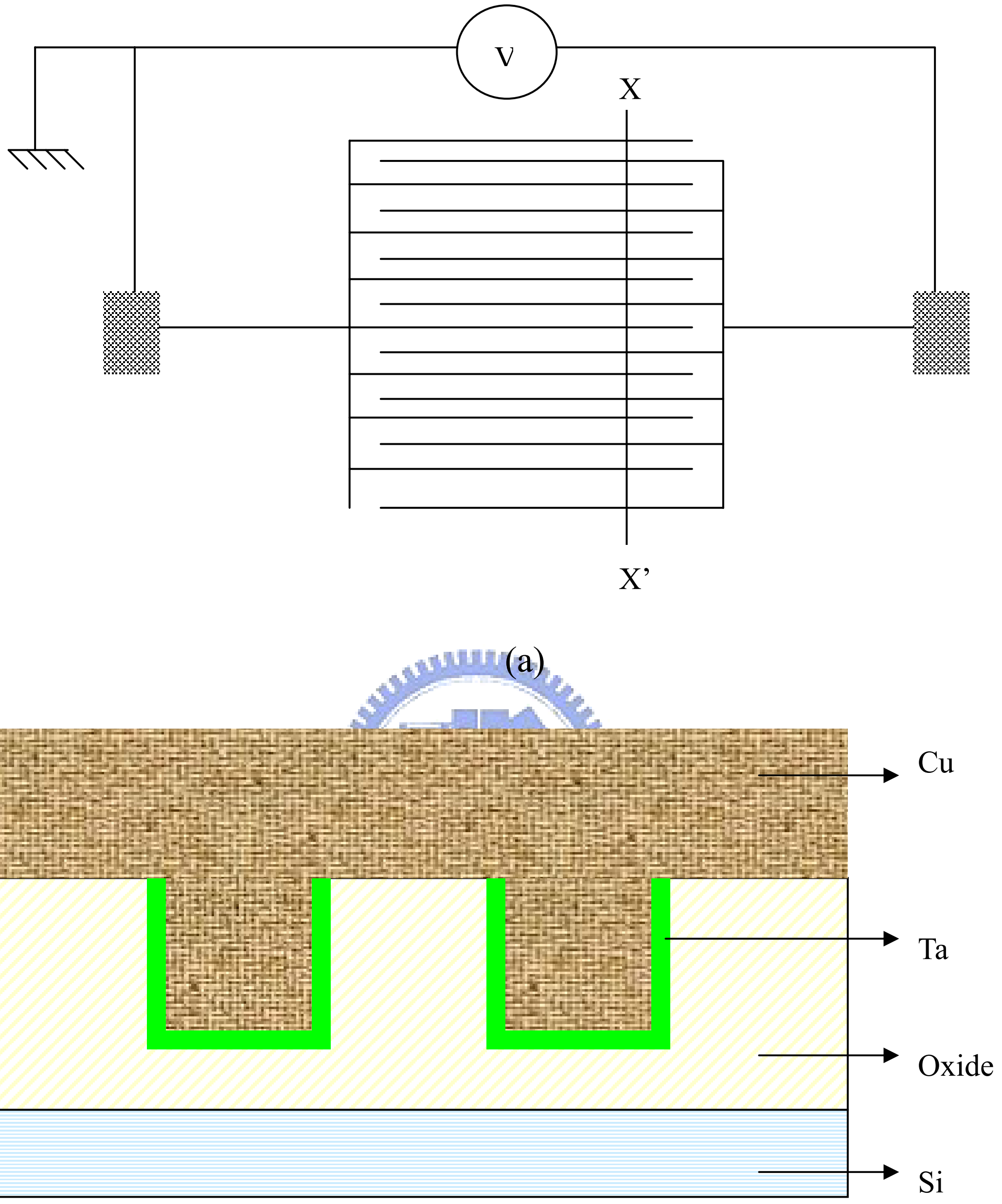

(a)

(b)

Figure.3-3 (a) Comb-line capacitor structure
(b) cross-section of comb structure.

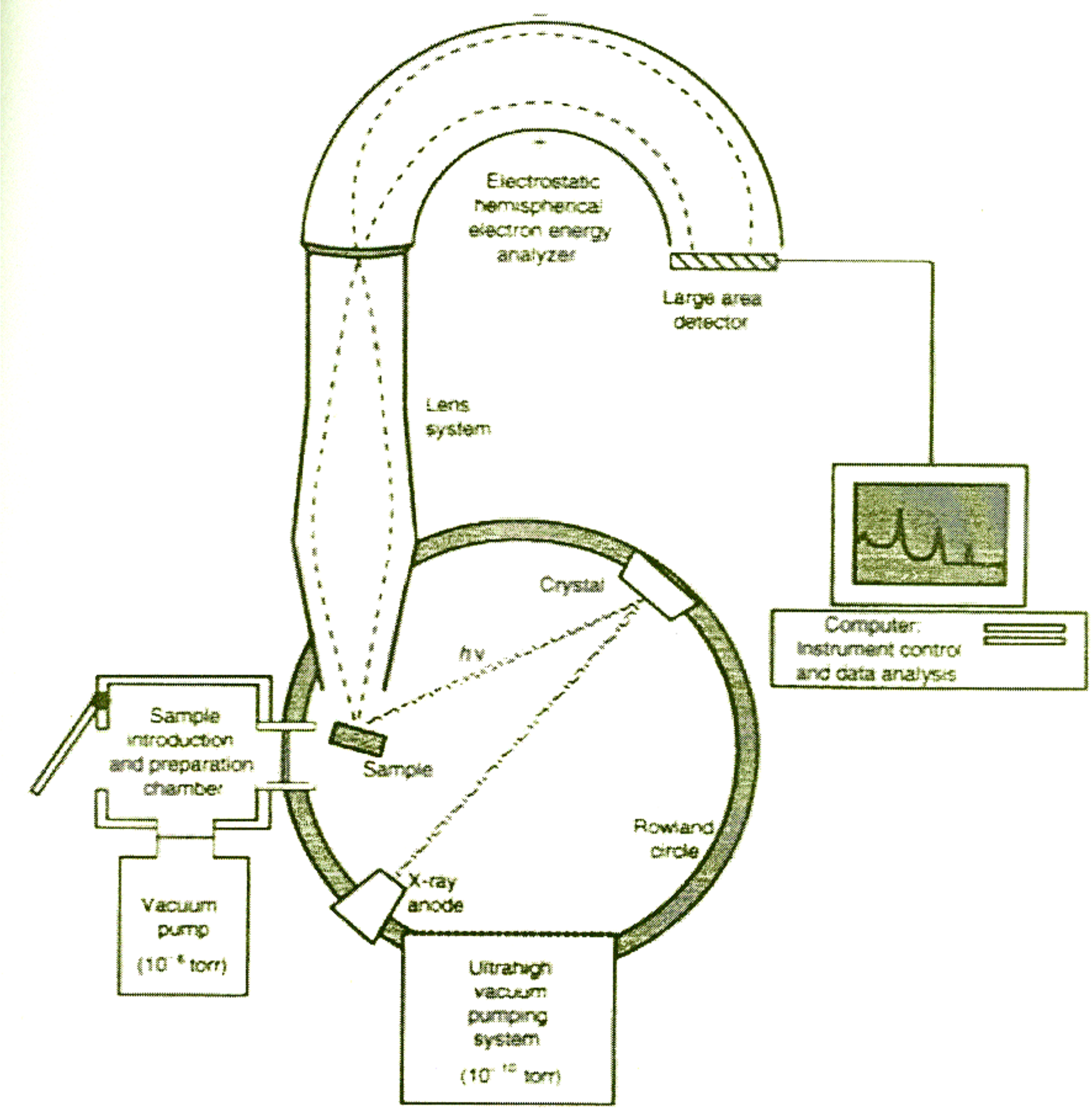

Figure.3-4 A schematic diagram of an ESCA spectrometer.

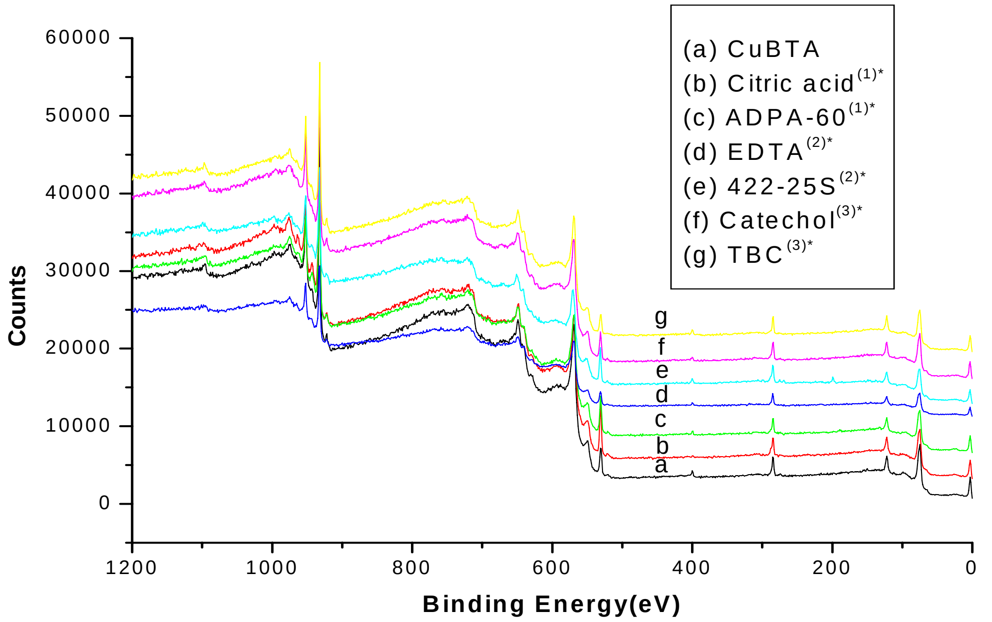

(a)

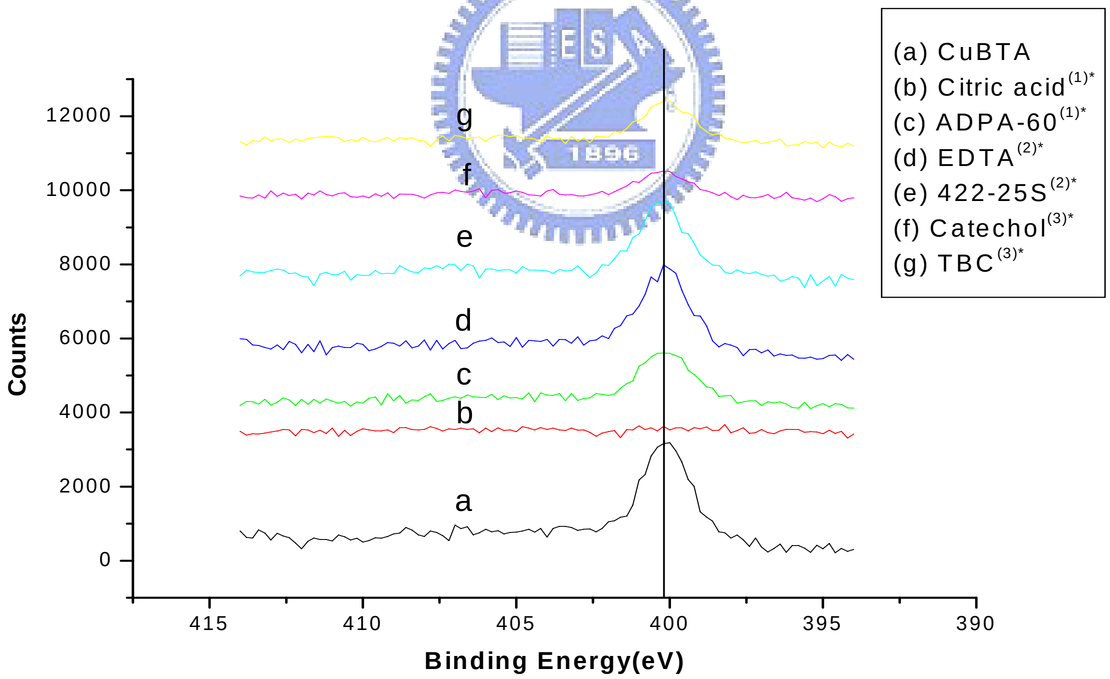

(b)

Figure.3-5 ESCA analysis of CuBTA after immersing of chelator solutions (a) Survey (b) Peak of N. *refer to the type of chelators.

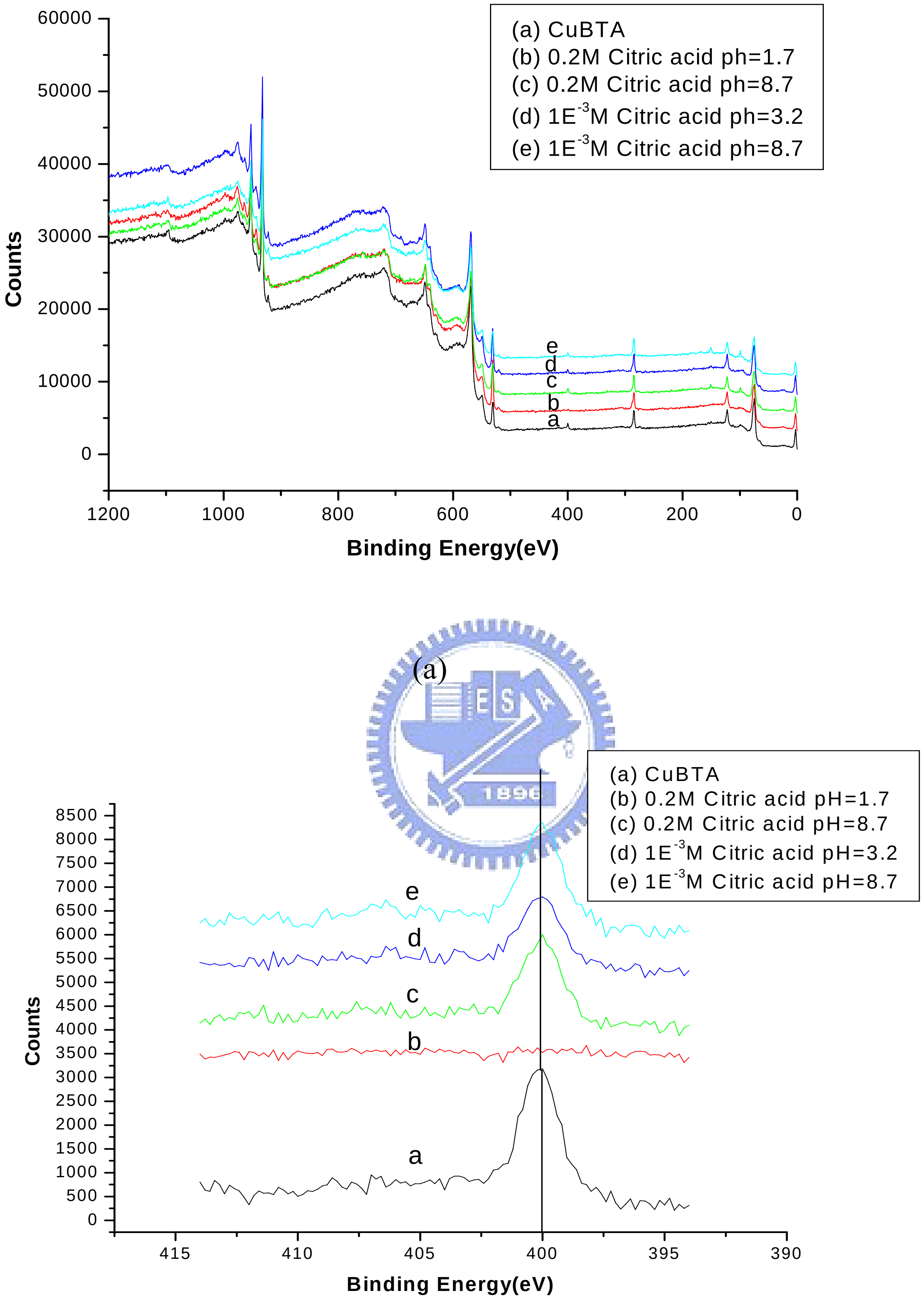

(a)

(b)

Figure.3-6 ESCA analysis of CuBTA after immersing of modified citric acid (a) Survey (b) Peak of N.

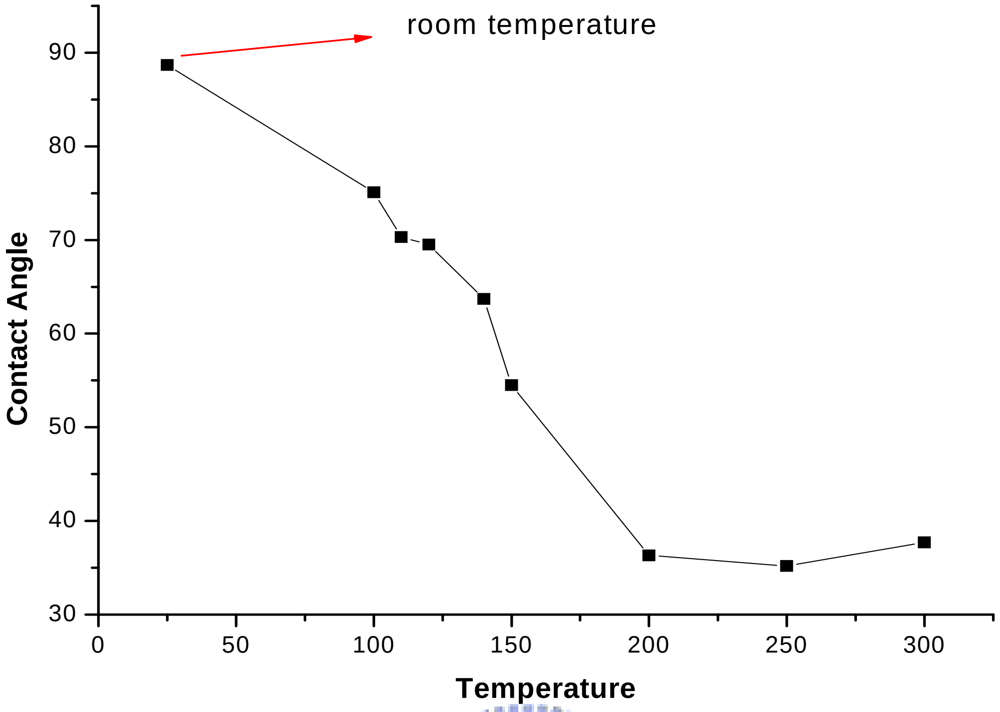

Figure.3-7 Contact angle analysis of temperature effect on CuBTA.

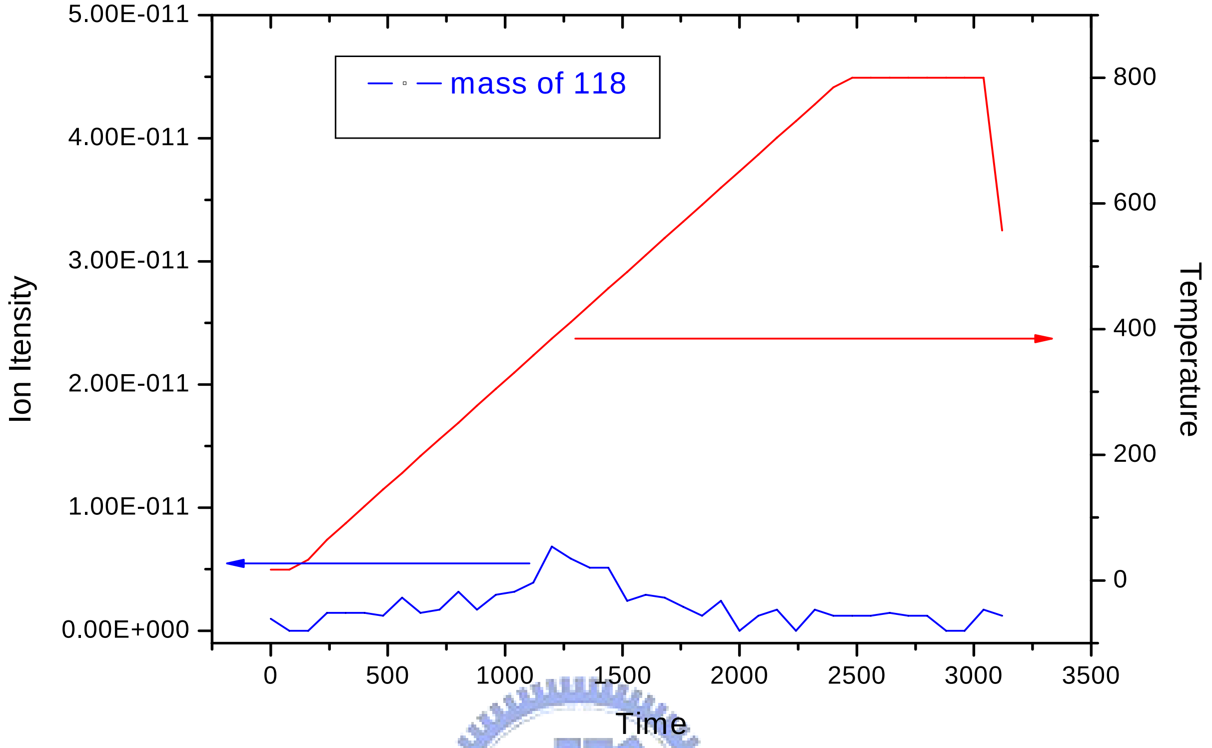

Figure.3-8 TDS analysis of temperature effect on CuBTA.

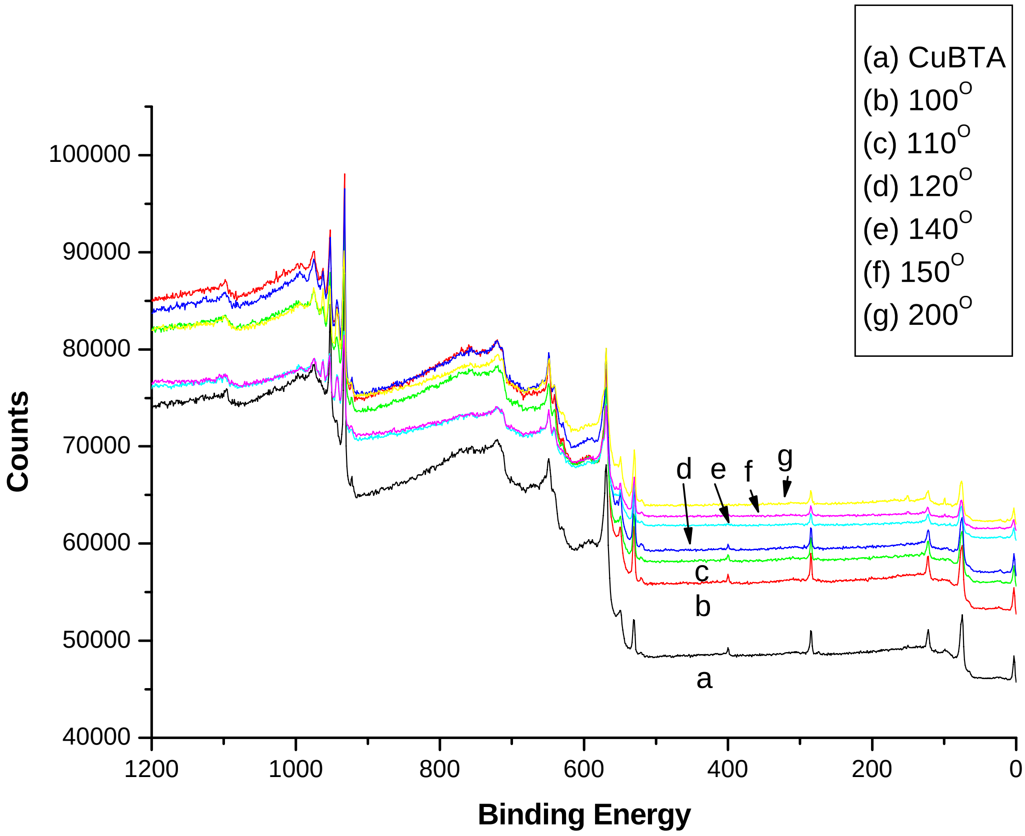
(a) CuBTA
(b) 100^{O}
(c) 110^{O}
(d) 120^{O}
(e) 140^{O}
(f) 150^{O}
(g) 200^{O}
Counts
100000
90000
80000
70000
60000
50000
40000
1200
1000
800
600
400
200
0
Binding Energy
d
e
f
g
c
b
a

(a)

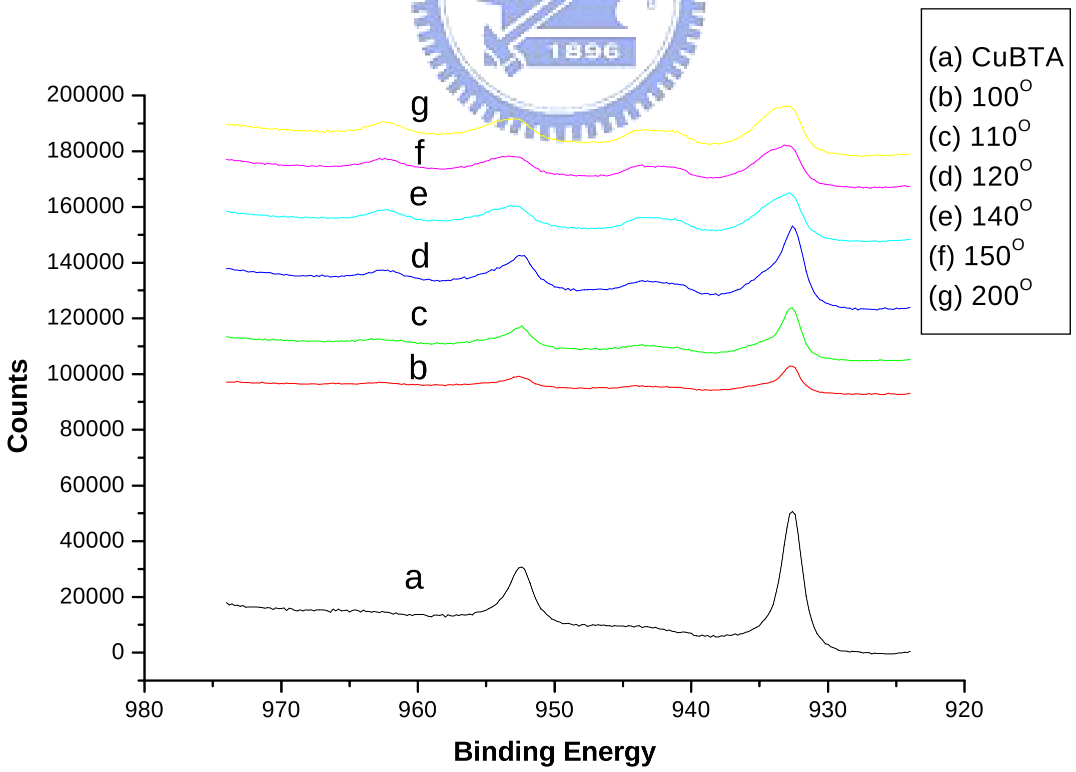
(a) CuBTA
(b) 100^{O}
(c) 110^{O}
(d) 120^{O}
(e) 140^{O}
(f) 150^{O}
(g) 200^{O}
Counts
200000
180000
160000
140000
120000
100000
80000
60000
40000
20000
0
980
970
960
950
940
930
920
Binding Energy
g
f
e
d
c
b
a

(b)

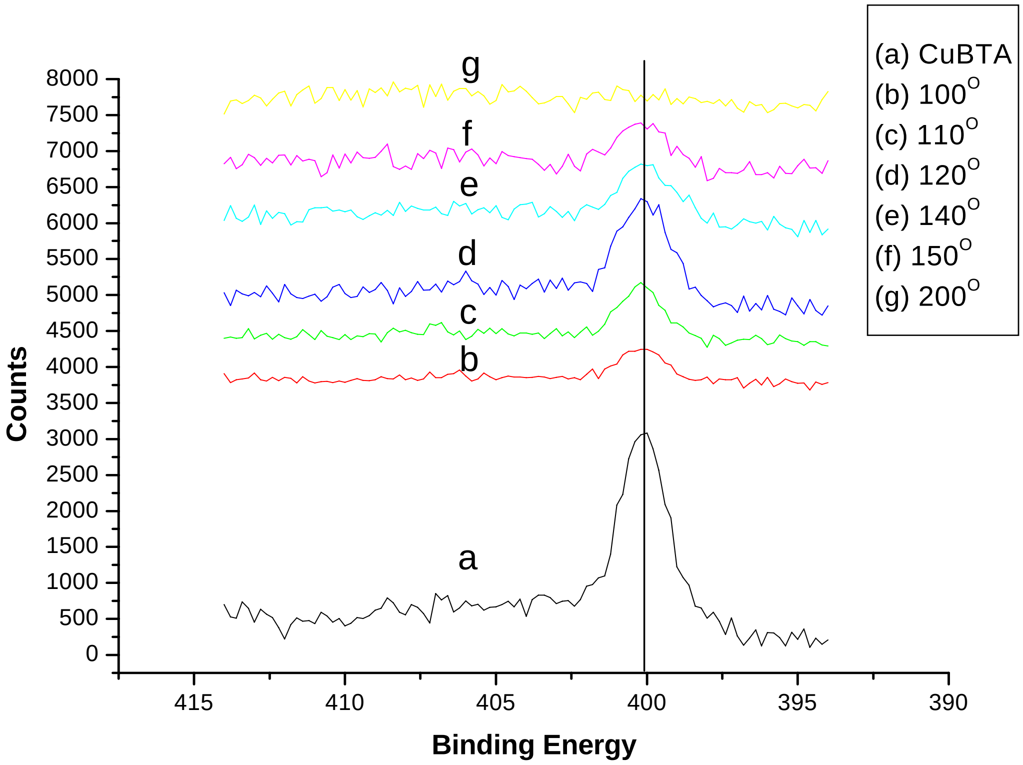

(c)

Figure.3-9 ESCA analysis of temperature effect on CuBTA (a) Survey (b) Peak of Cu (c) Peak of N.

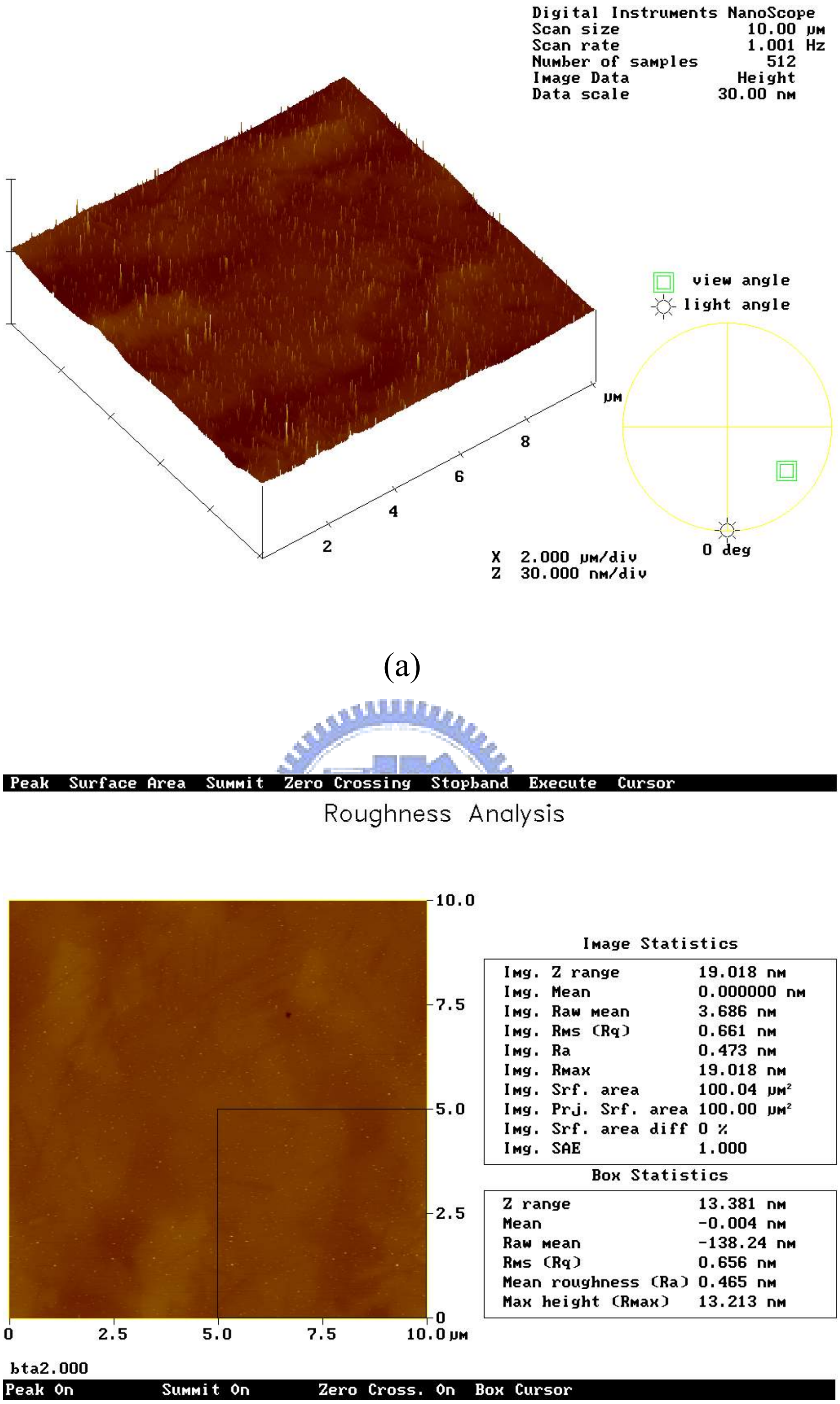

(a)

```
Image Statistics
Img. Z range          19.018 nm
Img. Mean             0.000000 nm
Img. Raw mean         3.686 nm
Img. Rms (Rq)         0.661 nm
Img. Ra               0.473 nm
Img. Rmax             19.018 nm
Img. Srf. area        100.04 µm²
Img. Prj. Srf. area   100.00 µm²
Img. Srf. area diff   0 %
Img. SAE              1.000

Box Statistics
Z range               13.381 nm
Mean                  -0.004 nm
Raw mean              -138.24 nm
Rms (Rq)              0.656 nm
Mean roughness (Ra)   0.465 nm
Max height (Rmax)     13.213 nm
```

(b)

Figure.3-10 AFM images of polished copper film with HNO_3/1H-BTA =0.6/1E^{-3}M, polishing time=1min (a) 3D diagram (b)roughness analysis.

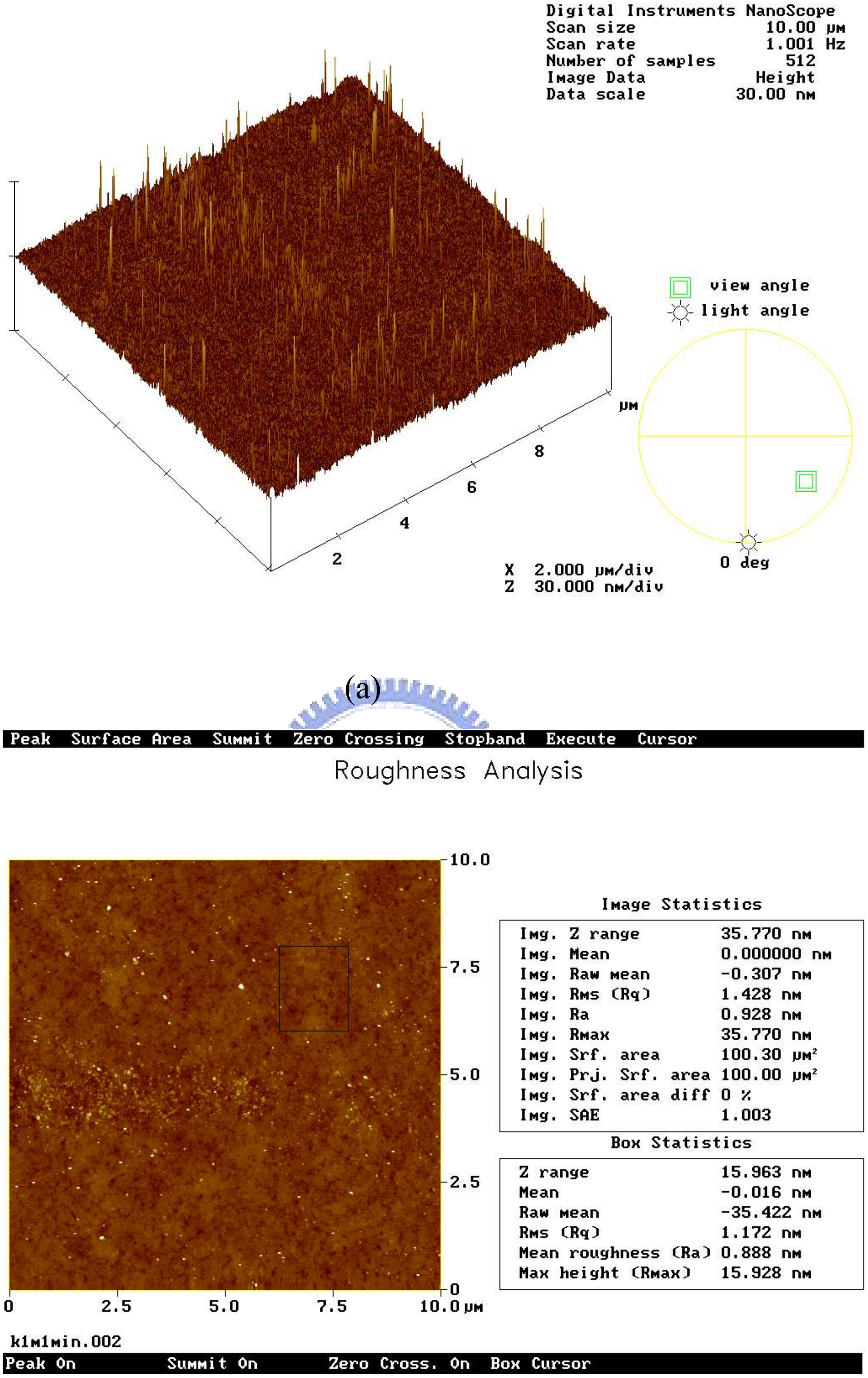

```
Digital Instruments NanoScope
Scan size              10.00 μm
Scan rate              1.001 Hz
Number of samples        512
Image Data             Height
Data scale            30.00 nm
```

```
X  2.000 μm/div
Z  30.000 nm/div
```

(a)

Image Statistics

Img. Z range	35.770 nm
Img. Mean	0.000000 nm
Img. Raw mean	-0.307 nm
Img. Rms (Rq)	1.428 nm
Img. Ra	0.928 nm
Img. Rmax	35.770 nm
Img. Srf. area	100.30 μm²
Img. Prj. Srf. area	100.00 μm²
Img. Srf. area diff	0 %
Img. SAE	1.003

Box Statistics

Z range	15.963 nm
Mean	-0.016 nm
Raw mean	-35.422 nm
Rms (Rq)	1.172 nm
Mean roughness (Ra)	0.888 nm
Max height (Rmax)	15.928 nm

k1m1min.002

(b)

Figure.3-11 AFM images of polished copper film with 1M KOH, polishing time=1min (a) 3D diagram (b)roughness analysis.

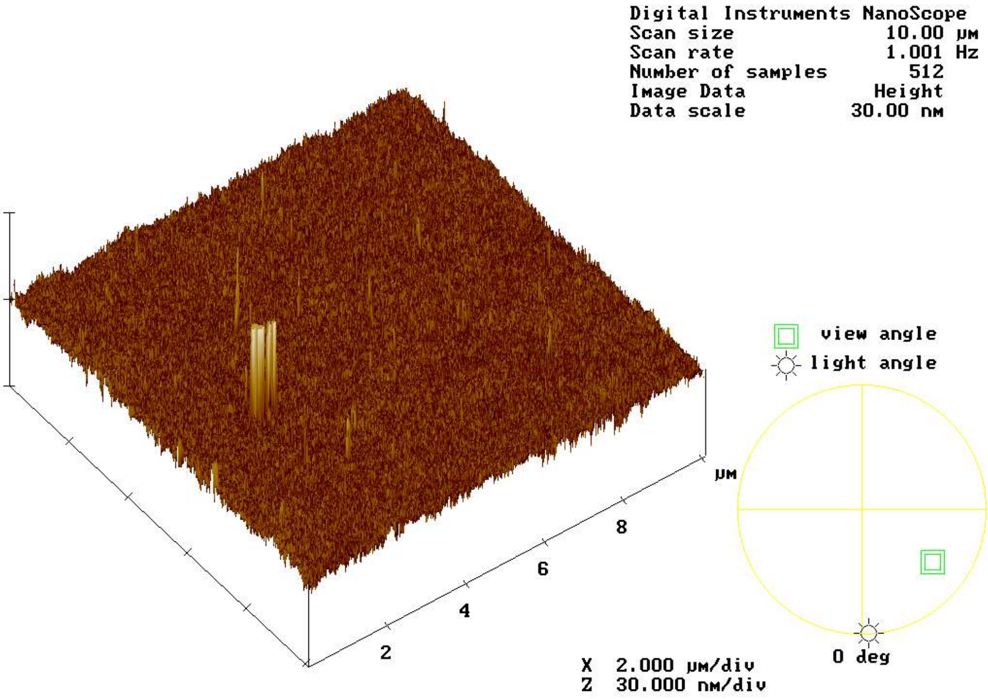

Digital Instruments NanoScope
Scan size 10.00 μm
Scan rate 1.001 Hz
Number of samples 512
Image Data Height
Data scale 30.00 nm

X 2.000 μm/div
Z 30.000 nm/div

(a)

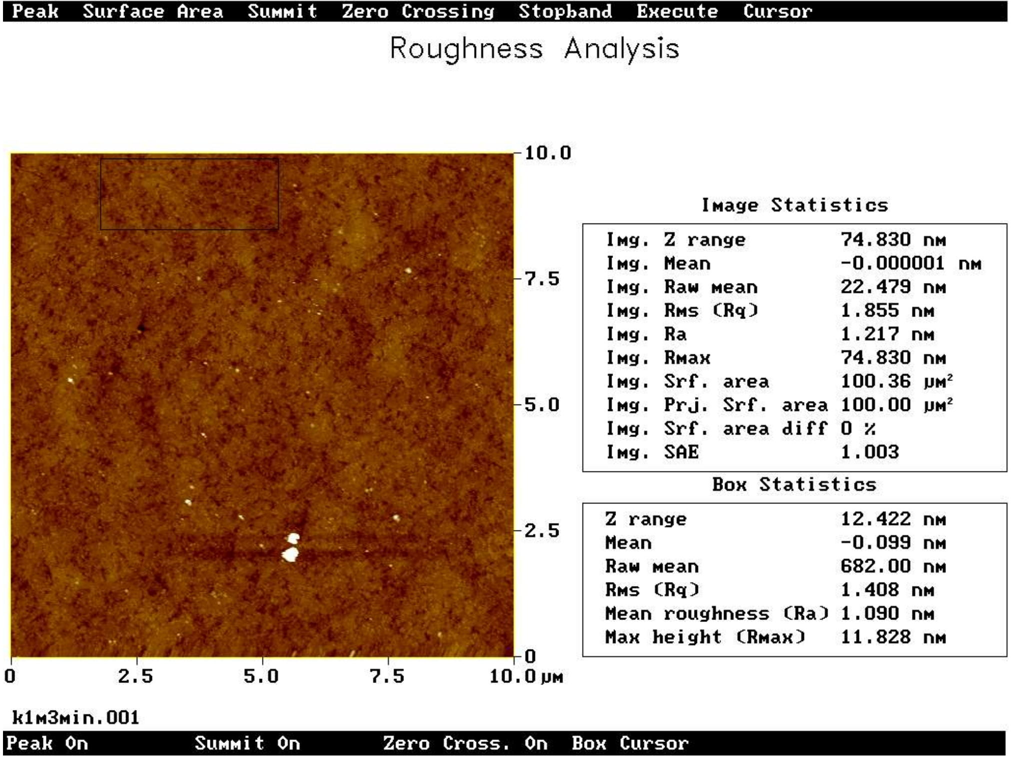

Roughness Analysis

Image Statistics

Img. Z range	74.830 nm
Img. Mean	-0.000001 nm
Img. Raw mean	22.479 nm
Img. Rms (Rq)	1.855 nm
Img. Ra	1.217 nm
Img. Rmax	74.830 nm
Img. Srf. area	100.36 μm²
Img. Prj. Srf. area	100.00 μm²
Img. Srf. area diff	0 %
Img. SAE	1.003

Box Statistics

Z range	12.422 nm
Mean	-0.099 nm
Raw mean	682.00 nm
Rms (Rq)	1.408 nm
Mean roughness (Ra)	1.090 nm
Max height (Rmax)	11.828 nm

k1m3min.001

(b)

Figure.3-12 AFM images of polished copper film with 1M KOH, polishing time=3min (a) 3D diagram (b)roughness analysis.

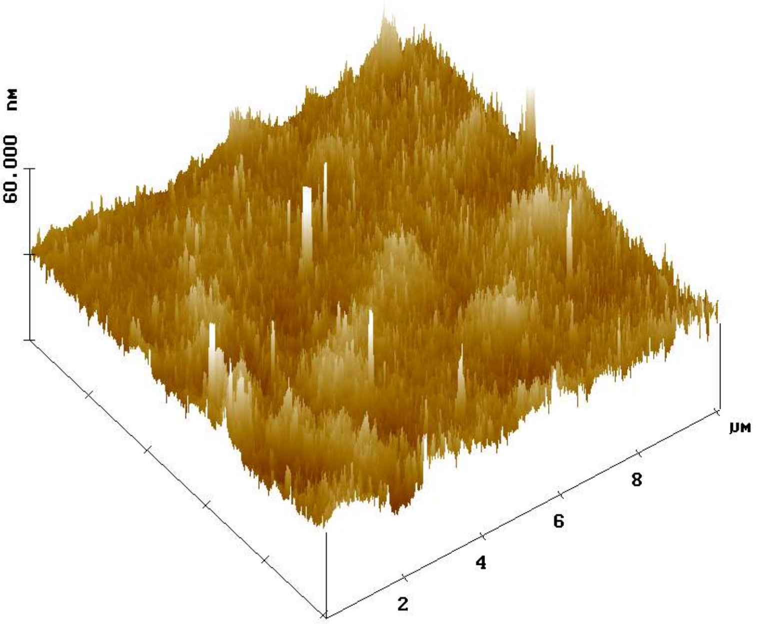

(a)

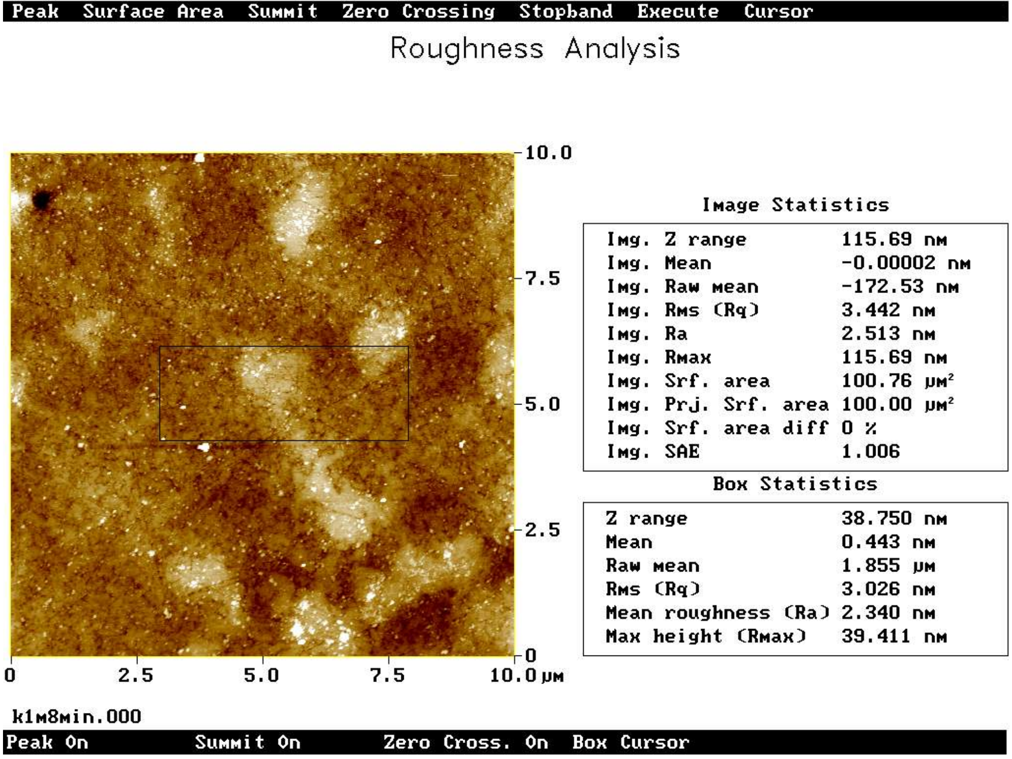

```
Roughness Analysis

              Image Statistics
Img. Z range            115.69 nM
Img. Mean               -0.00002 nM
Img. Raw mean           -172.53 nM
Img. Rms (Rq)           3.442 nM
Img. Ra                 2.513 nM
Img. Rmax               115.69 nM
Img. Srf. area          100.76 µM²
Img. Prj. Srf. area     100.00 µM²
Img. Srf. area diff     0 %
Img. SAE                1.006
               Box Statistics
Z range                 38.750 nM
Mean                    0.443 nM
Raw mean                1.855 µM
Rms (Rq)                3.026 nM
Mean roughness (Ra)     2.340 nM
Max height (Rmax)       39.411 nM

k1M8Min.000
```

(b)

Figure.3-13 AFM images of polished copper film with 1M KOH, polishing time=8min (a) 3D diagram (b)roughness analysis.

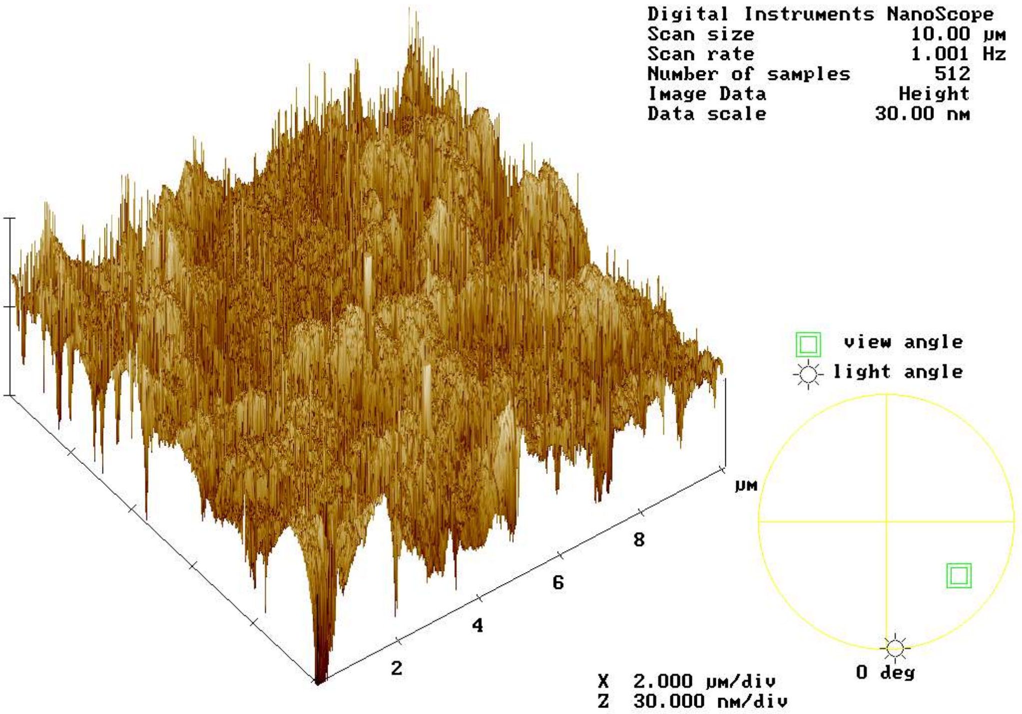

(a)

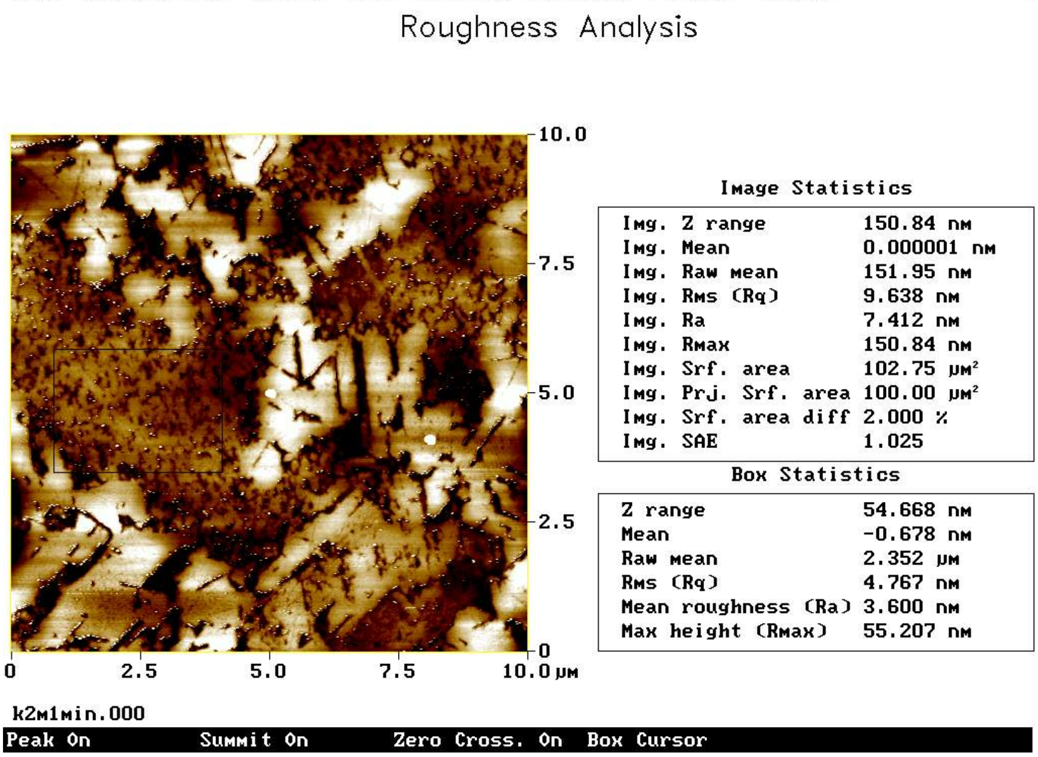

```
Image Statistics
Img. Z range           150.84 nm
Img. Mean              0.000001 nm
Img. Raw mean          151.95 nm
Img. Rms (Rq)          9.638 nm
Img. Ra                7.412 nm
Img. Rmax              150.84 nm
Img. Srf. area         102.75 µm²
Img. Prj. Srf. area    100.00 µm²
Img. Srf. area diff    2.000 %
Img. SAE               1.025
Box Statistics
Z range                54.668 nm
Mean                   -0.678 nm
Raw mean               2.352 µm
Rms (Rq)               4.767 nm
Mean roughness (Ra)    3.600 nm
Max height (Rmax)      55.207 nm
```

(b)

Figure.3-14 AFM images of polished copper film with 2M KOH, polishing time=1min (a) 3D diagram (b) roughness analysis.

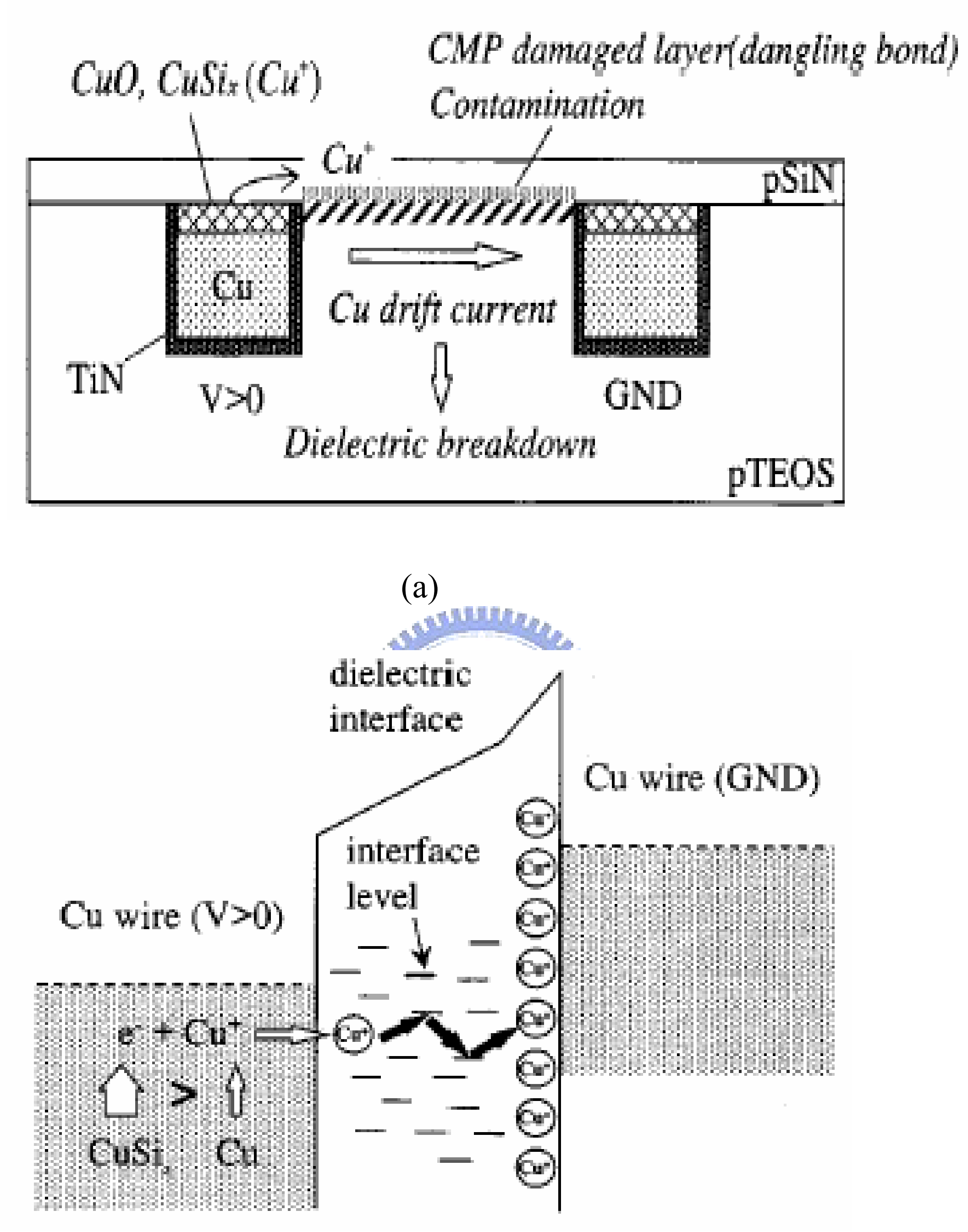

(a)

(b)

Figure.3-15 Mechanism of dielectric degradation
(a) TDDB degradation mechanism
(b) Band diagram of TDDB degradation.

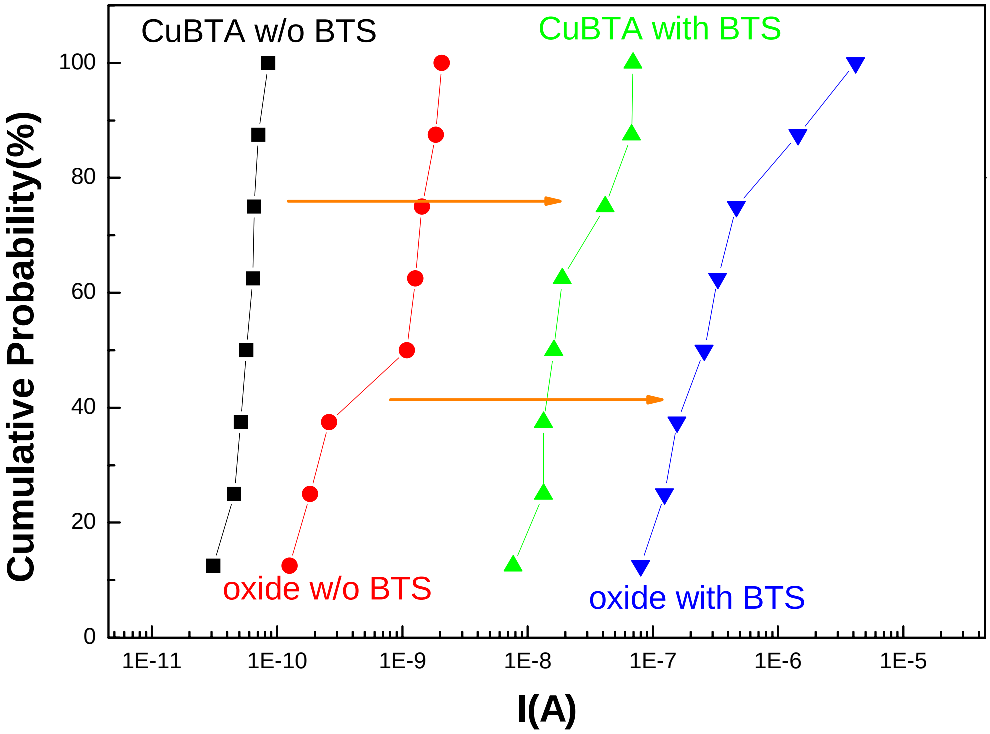

Figure.3-16 Plot of surface leakage property. (In plot, CuBTA meant CuBTA layer on surface of copper lines. Similarly, oxide meant Cu oxide on surface of copper lines. The current was measured at 90V.)

Vita

姓名：薛國欽
性別：男
出生年月日：民國 68 年 6 月 7 號
籍貫：台灣省高雄縣
通訊地址：高雄縣鳳山市北榮街 95 巷 4 弄 17 號
學歷：國立交通大學土木系
(民國 88 年 9 月至 民國 91 年 6 月)
國立交通大學電子工程所固態組
(民國 91 年 9 月至 民國 93 年 6 月)
碩士論文：化學機械研磨之清洗對銅導線電性的研究
Study on Eectrical properties of Cu Interconnect after Post CMP Cleaning